NUMERICAL SIMULATIONS OF THE FISH PASSAGE FACILITIES AT LOWER GRANITE DAM

by
Jeffery C. Blank and Larry J. Weber

Sponsored by
US Army Corps of Engineers
Walla Walla District Office
Walla Walla, Washington 99362

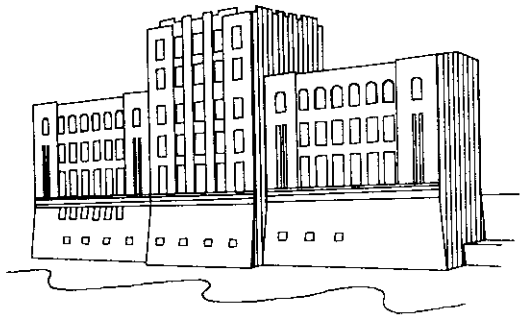

IIHR Technical Report No. 412

Iowa Institute of Hydraulic Research
College of Engineering
The University of Iowa
Iowa City, Iowa 52242-1585

November 2000

Report Documentation Page

Form Approved
OMB No. 0704-0188

1. REPORT DATE	2. REPORT TYPE	3. DATES COVERED
NOV 2000		**00-00-2000 to 00-00-2000**

4. TITLE AND SUBTITLE	5a. CONTRACT NUMBER
Numerical Simulations of the Fish Passage Facilities at Lower Granite Dam	5b. GRANT NUMBER
	5c. PROGRAM ELEMENT NUMBER
6. AUTHOR(S)	5d. PROJECT NUMBER
	5e. TASK NUMBER
	5f. WORK UNIT NUMBER
7. PERFORMING ORGANIZATION NAME(S) AND ADDRESS(ES) **The University of Iowa,College of Engineering,IIHR - Hydroscience & Engineering,Iowa City,IA,52242-1585**	8. PERFORMING ORGANIZATION REPORT NUMBER
9. SPONSORING/MONITORING AGENCY NAME(S) AND ADDRESS(ES)	10. SPONSOR/MONITOR'S ACRONYM(S)
	11. SPONSOR/MONITOR'S REPORT NUMBER(S)

12. DISTRIBUTION/AVAILABILITY STATEMENT
Approved for public release; distribution unlimited

13. SUPPLEMENTARY NOTES

14. ABSTRACT

15. SUBJECT TERMS

16. SECURITY CLASSIFICATION OF:			17. LIMITATION OF ABSTRACT	18. NUMBER OF PAGES	19a. NAME OF RESPONSIBLE PERSON
a. REPORT **unclassified**	b. ABSTRACT **unclassified**	c. THIS PAGE **unclassified**		**84**	

Executive Summary

The purpose of these numerical simulations is to investigate possible modifications to the fish diversion facilities currently installed at Lower Granite Dam. These modifications are intended to refine the flow field just upstream of the powerhouse thereby improving the juvenile salmonid attraction potential. A pressure-based finite volume, computational fluid dynamics code was utilized to solve the Reynolds-averaged Navier-Stokes equations. The computational grids, comprising between 350,000 and 1,000,000 nodes, simulated a region encompassing the entire dam geometry as well as 5000 feet upstream. This report describes the numerical model, model boundary conditions, numerical grid and general flow field dynamics obtained from the study as well as providing recommendations for future work pertaining to numerical studies of surface collection facilities.

Acknowledgments

The authors would like to thank Mr. Lynn Reese, US Army Corps of Engineers, Walla Walla District Office, for his guidance and support throughout this project. Also, thanks is given to Mr. Rolf Wielick, of Jacobs-Sverdrup, and Mr. Ken Hansen of CH2M Hill, Boise Office, for their assistance in contract administration of this work. The authors would also like to acknowledge Dr. John Nestler, from the Waterways Experiments Station in Vicksburg Mississippi, for his invaluable input towards this project.

Table of Contents

List of Tables

List of Figures

List of Nomenclature

Alphabetic Symbols

(a,b)	skewness diagonal lengths
ADV	acoustic doppler velocimeter
BGS	behavioral guidance structure
CFD	computational fluid dynamics
cfs	cubic feet per second
CG	conjugate gradient
DOE	United States Department of Energy
FGE	fish guidance efficiency
G	production term
k	turbulent kinetic energy
kcfs	thousand cubic feet per second
NMFS	National Marine Fisheries Service
P	pressure
PRP	Proposed Recovery Plan for the Snake River Salmon
PUD	public utility district
SBC	surface bypass and collection
SGI	Silicon Graphics Inc.
SIP	strongly implicit procedure
SOR	successive over-relaxation
SWI	simulated wells model insert
RANS	Reynold's averaged Navier-Stokes equations
t	time
U^2RANS	unsteady, unstructured Reynold's averaged Navier-Stokes
$\overline{u_i u_j}$	Reynolds stress tensor
USACE	US Army Corps of Engineers
WES	US Army Corp of Engineers Waterways Experiments Station
x_i	physical coordinates

Greek Symbols

$(C_{\varepsilon 2}, C_{\varepsilon 2})$	constants of the k-ε model
C_μ	constant of the k-ε model
δ_{ij}	Kronecker delta
ε	turbulent energy dissipation
$(\sigma_k, \sigma_\varepsilon)$	constant of the k-ε model
μ	dynamic viscosity
u_i	cartesian velocity component
μ_t	eddy viscosity

1. INTRODUCTION

The purpose of the numerical simulations presented in this report is to investigate possible modifications to the fish diversion facilities currently installed at Lower Granite Dam. These modifications are intended to refine the flow field just upstream of the powerhouse thereby improving the juvenile salmonid attraction potential. A pressure-based finite volume, computational fluid dynamics code is utilized to solve the Reynolds-averaged Navier-Stokes equations closed with the standard k-ε turbulence model. Four distinct computational grid arrangements were adopted for the simulation. Each topography was selected to optimize the solution accuracy around the surface collection facilities, while retaining efficient convergence times. In addition to the above details, this report will address the following key topics:

(i) Dependence of solution accuracy on grid detail;

(ii) Ability to efficiently model many different flow scales using the layered modeling approach;

(iii) Capacity to accurately capture the complex flow features found in a river/hydropower system;

(iv) Capabilities of computational fluid dynamics (CFD) as a design tool in fish passage; and

(v) Optimization of the super-BGS surface collection intake design to be constructed for 2000 testing.

Section 2 of this report focuses mainly on the procedures completed for generating the grids required to perform the numerical simulations. In addition, this section presents an overall

chronology of the research to date. Details of the numerical model algorithms as well as the calibration and validation procedure are addressed in Section 3. Section 4 presents the general results obtained together with a detailed description of the final surface collection entrance shape and hydraulic characteristics to be installed for 2000 prototype testing. Conclusions and recommendations for future research complete this report and are presented in Section 5.

2. GRID GENERATION

Numerical grid generation plays a critical role in many scientific computing problems, when the geometry of the underlying region is complex, or when the solution has a complex structure. The Lower Granite Dam fish collection facilities comprise such complex geometries thus making accurate and efficient grid generation difficult. The following section begins by presenting a general chronology of the research to date. This is followed by a discussion of the four major grids studied as well as some of the techniques utilized to increase their quality, efficiency and accuracy.

2.1. Model Chronology

Throughout the following section, readers should refer to figures 2.1 through 2.3 which, provide general overviews and illustrate the necessary terminology specific to Lower Granite Lock and Dam. Further details concerning Lower Granite Dam can be found in Appendix A of this report. The evolution of the numerical modeling of the fish collection and bypass facilities at Lower Granite Dam began in 1998 with a model that simply encompassed powerhouse units 4-6 as well as the surface collection system. A number of geometric modifications were explored including two curved extensions of different radii along the underside of the surface bypass and collection (SBC) gallery and a simulated Wells model insert (SWI), which attempted to reproduce similar hydraulic conditions to those present at Wells Dam. As this model evolved, the Behavioral Guidance Structure (BGS), a floating steel curtain designed to assist in guiding the juvenile fish into the surface collection system, was also integrated into the model. Numerous operational changes were also studied which included variations to both powerhouse loads and spill discharges as well as SBC opening configurations and operation. During the

course of these explorations, it became evident though, that more detailed grid refinement was required in the vicinity of the surface collection facilities as well as an overall larger spatial coverage. Furthermore, the results from the 1998 near-field model relied directly on physical model data for boundary conditions consequently limiting the test possibilities to those examined in the physical model. The enhancements to the model were made in 1999 and provided a greater ability to examine more detailed flow patterns as well as some of the larger scale effects.

The 1999 far-field model was utilized primarily as a tool to generate accurate boundary conditions for the more geometrically precise 1999 modified near-field model. This concept of separating the forebay into levels is called a layered modeling approach and is discussed later in this section. By incorporating the full extent of the forebay, the 1999 far-field model allowed all subsequent simulations to stand alone from physical model boundary data thereby eliminating the large cost and time constraints of physical modeling. The inlet boundary conditions for this model were produced from field data sets collected the previous year. All large-scale dam geometry was incorporated into this model with only slight simplifications present around the locking facilities and the upstream bank profile. It was shown through comparisons with field data that these simplifications had only minor localized effects and were not propagated through the remainder of the model. Future plans for this model include, amongst others, behavioral particle tracking whereby virtual fish are followed numerically throughout the domain.

The 1999 modified near-field model was built as a replacement for the 1998 near-field model and attempted to capture a larger section of the forebay in the vicinity of the powerhouse while still utilizing the same grid resolution. It is also the second level of the layered modeling approach and was used extensively in operational testing. The inlet boundary conditions were generated directly from the 1999 far-field model, and allowed for much more accurate boundary

conditions. Cross-validation was completed between both 1999 far and near field models to look for possible errors associated with grid refinement. This topic will be discussed in more detail later in this section.

Four primary operational configurations were studied using the new near-field model by varying the powerhouse discharge and surface bypass operation. It soon became evident though, that a smaller, denser, more efficient grid was required to look at actual design modifications to the interior geometry of the surface bypass facilities. Thus began the development of super near-field model, which is the third and final level of the layered modeling approach.

The 1999 super near-field model was constructed to analyze the flow phenomena at and inside of the SBC facilities. In this model, much of the structural framework was incorporated, with no significant geometric simplifications. With its boundary conditions generated in the modified near-field model, this arrangement was then used as a tool in the design process of the new super-BGS entrance, figure 2.4. Currently, four modifications have been tested using this model. Each idea was a derivation of its predecessor obtained by modifying entrance shapes to minimize turbulence and acceleration as the flow entered the unit. Results from these simulations are presented in Section 4 of this report.

2.2. Grid Generation Approach

Because of the limited number of previous three-dimensional simulations done within complex river-hydropower systems, many of the grid generation techniques required in this study were gathered from other disciplines of study. Gridgen™, a commercial mesh generation package, was used to generate the four multi-block, structured meshes which contained between 350,000 and 1,000,000 grid nodes. These general grid layouts were used throughout the study

with specialized modifications added when required. For more details concerning the Gridgen™ software package, readers are directed to Gridgen (1997).

Prior to any mesh generation, a structured grid topography was selected and adopted for the entire study. This scheme was chosen for two reasons. The first being that unstructured grid generation was not possible with the available Gridgen™ package, thus necessitating the purchase of new software or the development of a supplementary code. The second reason for selecting a structured grid arrangement was predominately based on computational efficiency. Each of the two numerical solvers, U^2RANS and FLUENT which are discussed in the next section, supports both structured and unstructured grids. Performance, however, is substantially faster for the structured arrangement. This is essentially due to the availability of different numerical linear equation solver algorithms. For unstructured grids, the only available solver is the robust, but relatively slow, conjugate gradient (CG) algorithm. For structured grids, on the other hand, more efficient solvers including SIP (Strongly-Implicit Procedure) and SOR (Successive Over-Relaxation) exist along with conjugate gradient. Use of structured grids provides the flexibility to utilize the faster solvers when the problem deems feasible while still having the availability to employ the robust CG algorithm. Performance gains for structured grids can also be obtained through the utilization of distinctly different data storage and accessibility routines (Lai, 1999).

To further illustrate the selection of a structured grid arrangement, grid density must be addressed. An efficient structured mesh can be generated quite rapidly using Gridgen™, while in this particular application, much time and effort must be given to generating an equivalently efficient unstructured mesh.

Due to the required relationship between complex geometry and the structured grid arrangement selected, a multi-block scheme was applied to accurately capture the entire physical domain, figure 2.5. The multi-block mesh approach was also utilized in order to obtain a detailed representation of the hydrodynamics near the dam while still remaining computational efficient. This gain in efficiency was achieved through a gradual expansion of the grid cell aspect ratio, increasing with distance upstream and laterally from the powerhouse region.

2.3. General Grid Overview

Before any discussion of the grid framework or quality characteristics can be undertaken, it is necessary to provide a more detailed description of the four main models: 1998 near-field model, 1999 far-field model, 1999 modified near-field model and 1999 super near-field model. The following section will briefly illustrate some of the major characteristics exhibited in each of the grids in addition to general size and topographical information.

The original 1998 near-field model, figure 2.6, which extended 200 feet upstream into the forebay, encompassed the area occupied by powerhouse units 4-6, the north, middle and south surface collection openings, and the behavioral guidance structure (BGS) curtain. The model contained approximately 500,000 grid points. A number of geometric simplifications were utilized for this model and will be discussed in section 2.5.

The 1999 far-field model, figure 2.7, incorporated a 5000-foot upstream reach from the face of the dam and modeled the entire width of the river. Actual 100-foot bathymetric cross-sectional information along with the spillways, surface collection gallery, locking facilities and overall powerhouse geometry was included. The resulting size if the 1999 far-field grid was

approximately 900,000 nodes. Later models included the BGS curtain as well as certain enhancements in the lock and SBC vicinity.

The 1999 modified near-field model, figure 2.8, was similar to the 1998 near-field model yet incorporated a larger overall spatial coverage. Encompassed in this model were powerhouse units 1-6 and spillways 1 and 2 as well as 50-foot bathymetric cross-sectional data extending 300-feet upstream. The most substantial addition to the 1999 near-field model, however, was the inclusion of the actual interior geometry of the surface collection gallery. Only a coarse representation of this geometry could be achieved because of the high grid densities required to accurately capture the flow field inside the SBC gallery and the limited availability of the necessary grid points. The 1999 modified near-field model contained approximately 1,000,000 grid points.

The final grid, the 1999 super near-field model, figure 2.9, established its boundaries 150-feet upstream of the dam face, 50 to the north and south of the middle and BGS surface bypass entrances respectively and 75-feet below the water surface. All major geometries were incorporated including the surface collection gallery floatation, the structural members bisecting the entrances and the interior entrance shape modifications. A more detailed description of the varying entrance shapes can be found in Section 4. Collectively, the entire model consisted of approximately 450,000 grid nodes depending on entrance shape geometry.

2.4. Simplifications

Inherent to almost any computational fluid simulation are simplifications to the physical geometry. Because of the extent of time by which this research was completed and the increase in computing speeds, physical geometry simplifications generally decreased throughout the

project. Nonetheless, the simplifications will be presented separately for each successive grid configuration, beginning with the 1998 near-field model and concluding with the most comprehensive 1999 super near-field model.

The 1998 near-field model contained the most significant simplifications of the four grids. These included modeling the river bathymetry as a smooth, constant slope bed, and completely excluding any details of the interior of the surface collection gallery. Figure 2.10 depicts the actual difference existing between the true bathymetric profile and the simplified constant slope bed representation. Additional, but less substantial simplifications involved neglecting structural members in and around the SBC openings, along with treating the pier geometry separating the powerhouse entrances as a vertical wall rather then including the actual slope, figure 2.11.

As in the 1998 near-field model, the 1999 far-field model included simplifications, however, the bulk of these changes were not located in the vicinity of surface collectors or powerhouse intakes and thus presented less difficulty in obtaining accurate results in the domain of interest. All dam and forebay geometry was incorporated into this model with only substantial simplifications present around the locking facilities and the upstream bank profile. Figure 2.12 highlights these river bank simplifications. The inaccuracies apparent here are a direct result of stretching the grid cells longitudinally away from the dam. When examining the results in the near forebay, however, it can be shown that these simplifications did not significantly affect the accuracy of the solution. Because of the large overall coverage encompassed in the 1999 far-field model, coarse grid densities were inherent throughout and inhibited the ability to capture any of the structural geometry associated with the surface collection intakes. This, naturally, forced the exclusion of the interior SBC geometry.

The 1999 modified near-field model contained only minor simplifications near and inside of the surface collectors, however, because it encompassed such a large area and, consequently, required an extremely large amount of grid points, it was computationally slow. The overall topography of the grid, nevertheless, was sufficient and this model produced quite rapid convergence rates given the large overall node count.

Excluded in the 1999 modified near-field model were the SBC floatation box, some of the small-scale structural members separating the SBC entrance weir and the actual interior SBC gallery geometry. The inability of the 1999 modified near-field model to capture the true SBC gallery shape was a direct result of the limited grid densities along the intake weir. This inhibited the model's ability to incorporate many of the small fillets and radii thus generating an inaccurate representation of the flow field inside of the SBC gallery.

The most comprehensive of the four models was the 1999 super near-field model. This grid included much of the structural framework in an attempt to eliminate any significant simplifications. Because the vast majority of the dam geometry was included in this model, subsequent errors were more likely a result of insufficient boundary conditions or the application of a steady-state solution rather than a true unsteady simulation.

2.5. Grid Quality

The quality embodied in a grid will directly affect solution time and accuracy. This issue becomes most evident during extreme cases of inadequate grid quality, which result in computational divergence. The following three sub-sections will discuss grid quality issues at Lower Granite Dam with respect to skewness, cell aspect ratio and grid clustering.

2.5.1. Skewness

Cell skewness was undoubtedly the most problematical grid quality issue encountered at Lower Granite Dam. Figure 2.13a illustrates general cell skewness in two-dimensions. Skewness can be defined for a quadrilateral in two-dimensions as one minus the ratio of the shorter diagonal of the element divided by the remaining diagonal.

$$\text{Cell Skewness} = 1 - \left(\frac{a}{b}\right)_{a<b} \tag{2.1}$$

A cell skewness of near 0 corresponds to an entirely orthogonal cell while values approaching 1.0 represent a highly skewed or collapsed cell. The concept of cell skewness as applied to the current Lower Granite simulations was computed for each three-dimensional element using vertex normals, figure 2.13b, rather than diagonals, however, the resulting ratios were equivalent to the two-dimensional case.

High levels of cell skewness were most evident in the Lower Granite grid along the riverbank line where the bottom bathymetric cross sections and the water surface converge to a point. Initial grid generation schemes attempted to break the bathymetric cross-sections about 50-feet from either end and generate a domain using the three newly created sides along with the water surface, figure 2.14a. The resulting domain generally exhibited high cell skewness levels adjacent to the imposed break points and resulted in the propagation of this feature throughout the remainder of the block. Without substantial relaxation applied to the turbulence and momentum equations, a divergent solution was attained using this method.

To reduce the overall skewness caused by this scheme a new method was adopted. In essence, the new method divided the domain by adding a small, 2-foot vertical connector at either end of the water surface, which joined to the riverbed, rather than at some arbitrary break

point alone the bathymetric cross-sections. Grid point spacing was then prescribed equivalently along both the riverbed cross-sections and water surface thus producing a domain with minimally skewed grid cells, figure 2.14b. Ideally, a pole connector would replace the 2-foot vertical lines, thus converging to a true point, however U^2RANS could not accept this topological scheme.

After acceptable levels of skewness were achieved along all boundary domains the interior cells were generated. An elliptical solver provided by Gridgen™, which is essentially a smoothing filter, was then applied to the interior points enhancing the overall cell orthogonality. The interested reader is directed to Gridgen (1997) for a more comprehensive description of the elliptical solver.

2.5.2. Cell Aspect Ratio

The ratio of the longitudinal cell length to the transverse length defines cell aspect ratio in two-dimensions.

$$\text{Aspect Ratio} = \left(\frac{\Delta x_i}{\Delta x_j} \right)_{i \neq j} \tag{2.2}$$

Because both numerical algorithms utilized during this research employed a finite volume discretization scheme, the cell aspect ratio was not the predominate influence in convergence time or solution accuracy. To maintain a high level of grid quality, however, large cell aspect ratios were limited to regions where the solution accuracy was less crucial. Near the surface collection entrances, cell aspect ratios near 1:1 in all directions were maintained. As the domain extended upstream away from the dam as well as laterally north from the locking facilities, the cell aspect ratio was stretched considerably to levels approaching 1:50 in the horizontal plane. Even with these high levels of stretching, however, an accurate, converged solution was readily obtained.

2.5.3. Grid Clustering

To resolve the complex flow phenomena in and around the surface collectors, grid point clustering was utilized. By concentrating a high number of nodes around the SBC entrances, more detailed flow features were captured. This high grid density also allowed for the inclusion of more complex geometries as in the 1999 super near-field model. Grid clustering was also adapted more sparingly in the vicinity of the powerhouse intakes and the behavioral guidance structure (BGS) curtain. In locations where detailed flow features were not required, grid point separation was dramatically increased to reduce solution times. Figure 2.15 illustrates a representative selection of both high and low levels of grid clustering.

2.6. Layered Modeling Methodology

A layered model approach was adopted for the 1999 test cases in which three successively finer grids were constructed and solved, beginning with the full far-field model and concluding with the super near-field model. This technique was chosen by virtue of two incentives, the first being to utilize the coarse models primarily as a tool to generate accurate boundary conditions for the more geometrically precise fine scale grids. Essentially, the 1999 far-field model was utilized to generate boundary conditions for the 1999 modified near-field model, which was, in turn, was used to generate boundary conditions for the 1999 super near-field model. The second incentive was to produce an accurate solution of the varying spatial flow scales while still maintaining computational efficiency.

The layered modeling approach has been utilized in many diverse fields including coastal models and atmospheric simulations to name a few. With today's computational hardware and numerical algorithms, the layered modeling approach benefits far outweigh the cost of

necessitating three separate grid domains and solutions. With future enhancements being researched in areas of arbitrary block interfacing along with performance enhancements for an unstructured grid topology, the layered modeling methodology may be replaced with a single grid in the future.

2.7. Summary

This section presents issue concerning grid generation and its quality assurance. Grids maintaining low levels of skewness and cell stretching along with appropriate grid clustering will undoubtedly increase convergence rates and solution accuracy. All of the above features were incorporated into each of the Lower Granite Dam grids and in conjunction with the layered modeling methodology, produced quite accurate results. The following section presents the details of the numerical model along with a discussion of the model calibration and validation procedure and results.

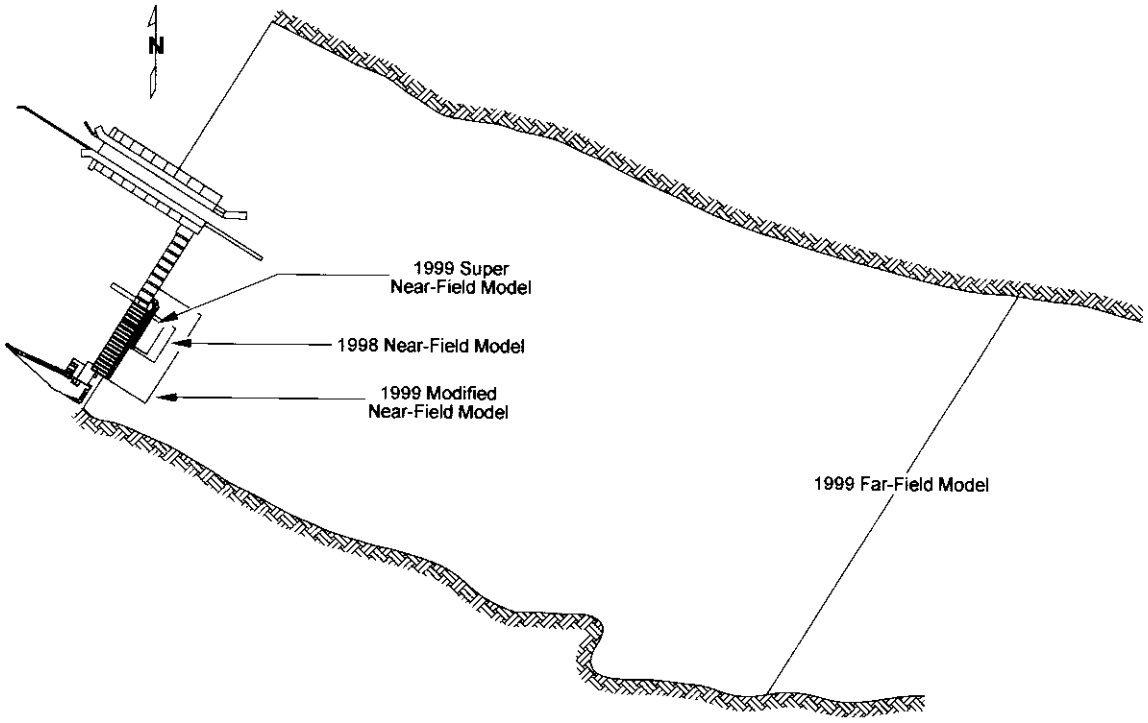

Figure 2.1 Boundaries of the four numerical models for Lower Granite Lock and Dam.

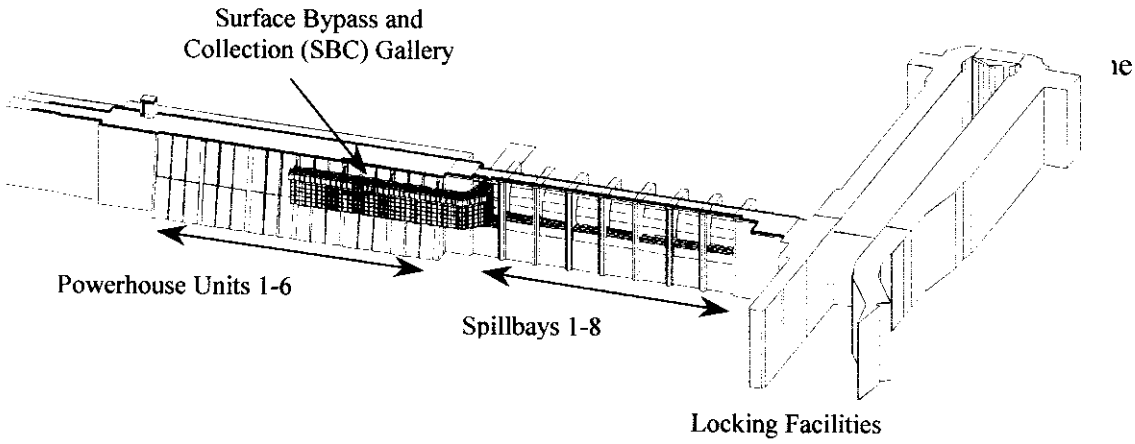

Figure 2.2 Identification of the pertinent structural components of Lower Granite Lock and Dam.

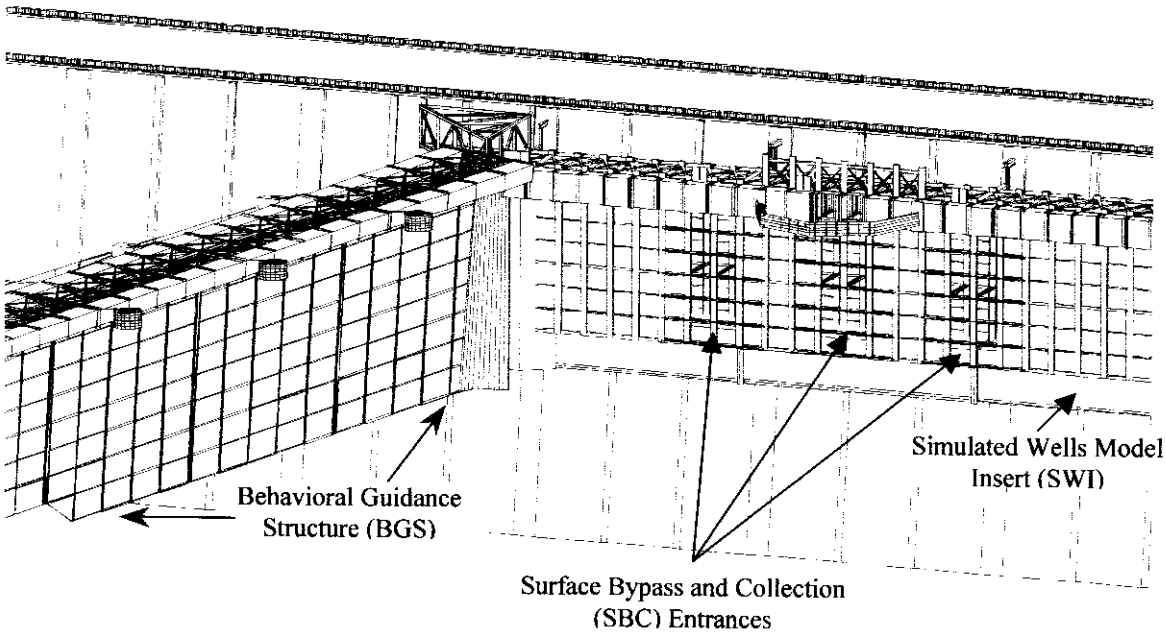

Figure 2.3 Detailed representation of the Behavioral Guidance Structure (BGS), the Simulated Wells Model Insert (SWI) and the Surface Bypass and Collection (SBC) entrances.

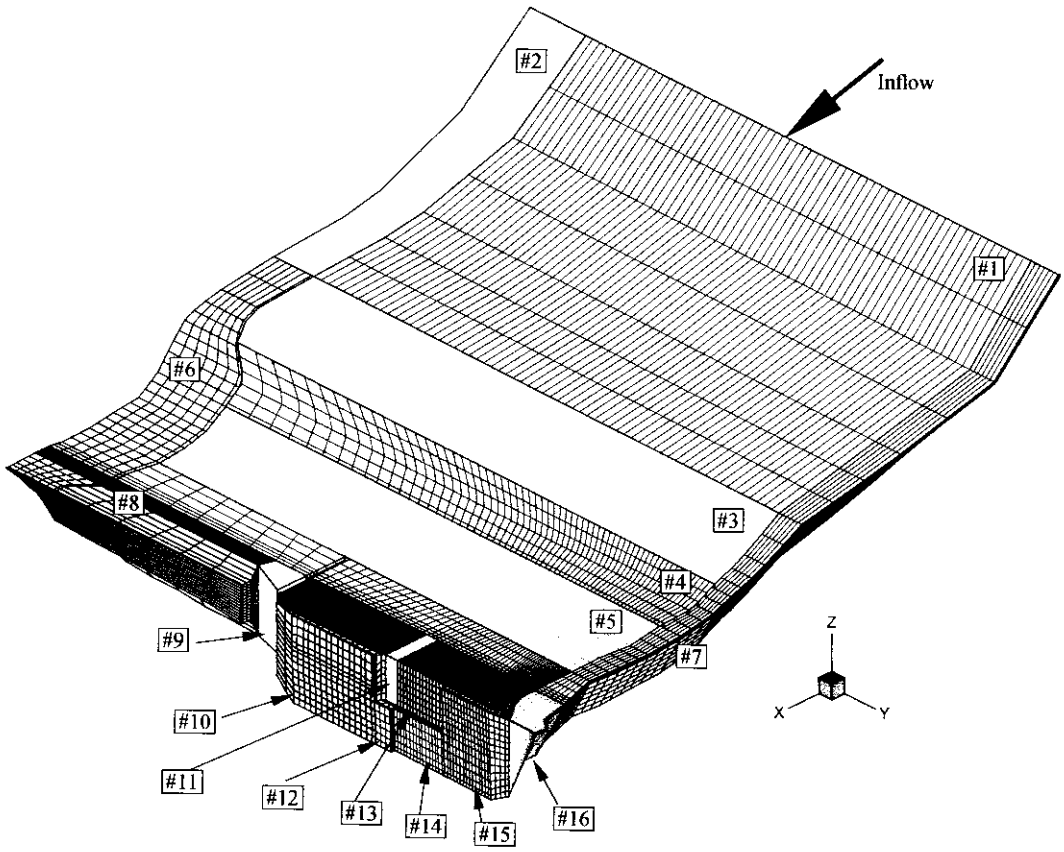

Figure 2.5 Representative schematic of the multi-block grid arrangement utilized throughout the Lower Granite Lock and Dam numerical model.

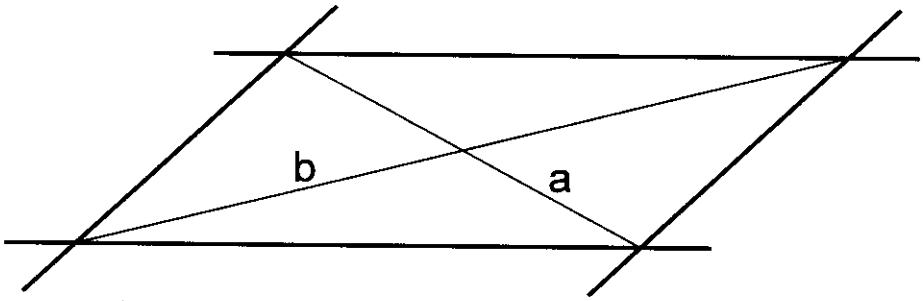

a) General skewness in two-dimensions using cross-diagonal lengths

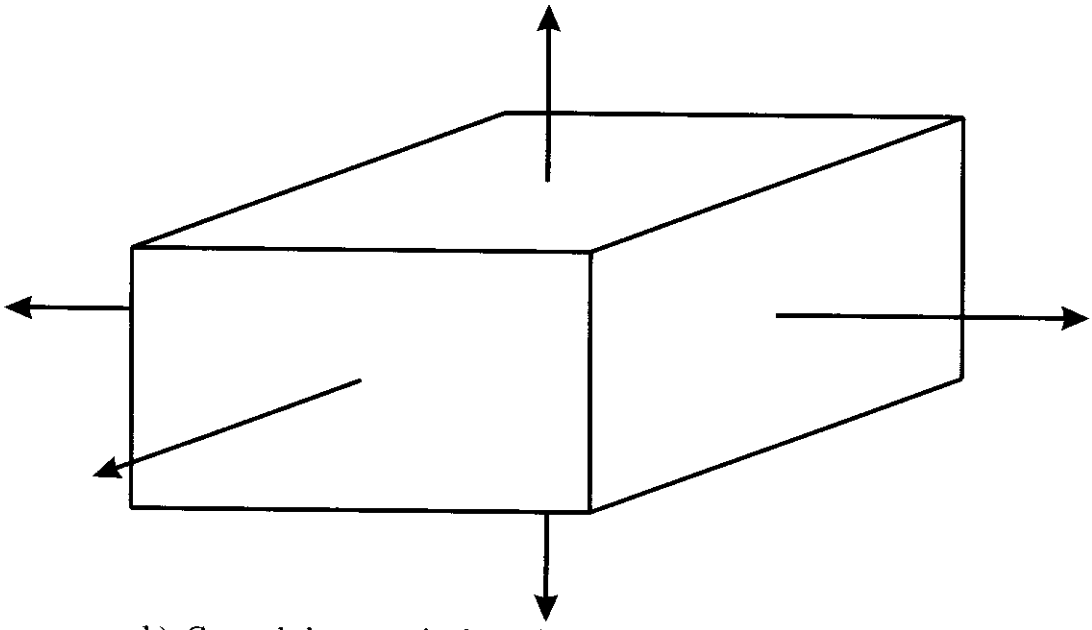

b) General skewness in three-dimensions using vertex normals

Figure 2.13 Schematic of the general method for computing skewness in both two and three-dimensions.

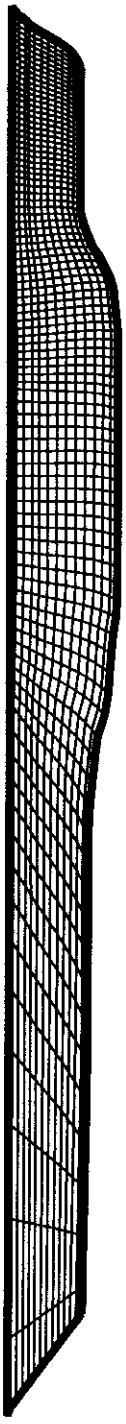

a) Original highly skewed river cross-section

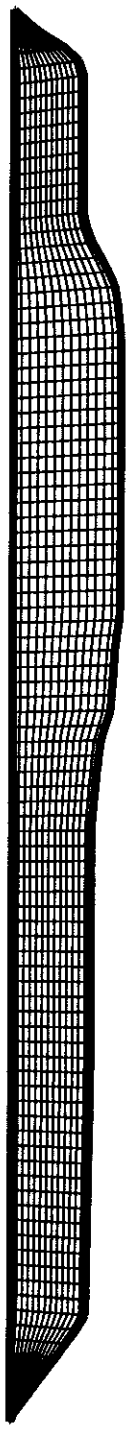

b) Final river cross-section with minimal skewness

Figure 2.14 Illustration of representative river cross-sections with high and low levels of skewness.

3. NUMERICAL MODEL CALIBRATION AND VALIDATION

The following section presents the details of the numerical model as well as the boundary conditions, convergence requirements, calibration and validation. Because code development was beyond the scope of this research, a consolidated description of the numerical model will be presented with appropriate references. This will be followed by a more rigorous description of the applied boundary conditions and convergence criteria. The calibration and validation of the four models will then be addressed, with emphasis on the 1998 near-field model as well as cross-validation of the 1999 models.

3.1 Numerical Model

The governing equations for turbulent, incompressible fluid flow are the Reynolds averaged Navier-Stokes (RANS) equations closed with a suitable turbulence model. This study utilized a CFD code currently being developed by Lai (1999) at the Iowa Institute of Hydraulic Research (IIHR). The basis of this code is a finite-volume numerical method for solving the three-dimensional RANS equations, in conjunction with the k-e turbulence model. The following section will provide an overview of the general equations of motion being solved together with the turbulence closure model. For a more rigorous description of the code architecture and numerical methods, see Lai (1999) and Lai (1999).

3.1.1. Governing Equations

The conservation of mass and momentum can be characterized through the following set of Cartesian equations (tensor form):

Continuity equation:

$$\frac{\partial(\rho U_j)}{\partial x_j} = 0 \tag{3.1}$$

Momentum Equation:

$$\frac{\partial \rho U_i}{\partial t} + \frac{\partial(\rho U_i U_j)}{\partial x_j} = -\frac{\partial P}{\partial x_i} + \frac{\partial}{\partial x_j}\left(\mu \frac{\partial U_i}{\partial x_j} - \rho \overline{u_i u_j}\right) \tag{3.2}$$

where U_j and u_j are the j-th components of the mean and fluctuating velocities, P is the mean pressure, and ρ and μ are the fluid density and viscosity, respectively.

3.1.2. Turbulent Closure Equations

In the above equations, a turbulence model is needed for the Reynolds stress term $\overline{u_i u_j}$. An isotropic eddy-viscosity model was utilized, namely, the standard k-ε model (Launder and Spalding, 1974). In this model, the Reynolds stresses are related to the mean rate of strain through an eddy viscosity;

$$-\rho \overline{u_i u_j} = \mu_t \left(\frac{\partial U_i}{\partial x_j} + \frac{\partial U_j}{\partial x_i}\right) - \frac{2}{3}\rho k \delta_{ij} \tag{3.3}$$

and eddy viscosity is obtained from

$$\mu_t = C_\mu \rho \frac{k^2}{\varepsilon} \tag{3.4}$$

where k is the turbulence kinetic energy, and ε is the turbulence dissipation rate. The transport equation for k can be expressed as;

$$\frac{\partial \rho U_j k}{\partial x_j} = \frac{\partial}{\partial x_j}\left[\left(\mu + \frac{\mu_t}{\sigma_k}\right)\frac{\partial k}{\partial x_j}\right] + G - \rho\varepsilon \tag{3.5}$$

where $G = -\rho\overline{u_i u_j}(\partial U_i / \partial x_j)$ is the generation of k. The second transport equation involves ε and can be expressed as

$$\frac{\partial \rho U_j \varepsilon}{\partial x_j} = \frac{\partial}{\partial x_j}\left[\left(\mu + \frac{\mu_t}{\sigma_\varepsilon}\right)\frac{\partial \varepsilon}{\partial x_j}\right] + C_{\varepsilon 1}\frac{\varepsilon}{k}G - C_{\varepsilon 2}\rho\frac{\varepsilon^2}{k} \tag{3.6}$$

The k-e turbulence model coefficients are listed below:

C_μ=0.09, $C_{\varepsilon 1}$=1.44, $C_{\varepsilon 2}$=1.92, σ_k=1.0, σ_e=1.3

3.2. Boundary Conditions

For clarity in presentation, each separate category of boundary conditions will be discussed individually. Omitted in the following section is the presentation of the inlet conditions, which will be discussed subsequently under the experimental boundary conditions section. Readers are again referred to Lai (1999) for more details as to the actual numerical techniques being utilized at each boundary.

3.2.1. General Boundary Conditions

Three general boundary conditions were applied within each model. They included outlets, solid surfaces, and symmetry. Each is presented in the following sections.

3.2.1.1 Outlets

Specification of the outflow conditions was generally accomplished using a combination of constant discharge outlets and uniform pressure outlets. A uniform velocity was enforced at the required outlet planes to enforce an accurate mass flow rate through that plane. This was generally imposed on all but one outlet plane so as to not require precise accuracy of global continuity at all planes, thus allowing for the code to estimate through extrapolation, the

remaining discharge. The pressure field at the exit plane whose discharge was not specified is found through linear extrapolation from the interior domain.

3.2.1.2 Solid Surface

To avoid complexities in modeling the turbulent near-wall region, the two-point wall function (Chen and Patel 1988) was applied to all solid surface boundaries. A detailed description of this approach can be found in Sinha (1995). Because of code limitations, no boundary roughness was imposed. This assumption, however, has been shown to be satisfactory for large-scale river reaches whereby relatively large variations of the bed roughness resulted in minimal change in the general flow patterns. It should be noted that the inclusion of boundary roughness, nonetheless, could aid in fine tuning the calibration and validation agreement. (Sinha 1995).

3.2.1.3 Free Surface

The free surface is specified as a fixed flat smooth lid. The tangential velocity components at the free surface are found through extrapolation from the interior while the normal velocity is fixed to zero. The turbulence quantities and pressure field at the free-surface are also found through linear extrapolation from the interior of the computational domain. It should be noted that the plane of symmetry condition does not imply that water-surface changes are not present. However, in similar applications, where superelevations are small, the error introduced by using the symmetry assumption does not compromise the accuracy of the solution (Meselhe 1998).

3.2.2. Inlet Boundary Conditions

The velocity inlet boundary conditions are comprised of actual velocity measurements being prescribed at the inlet planes of the domain. This inlet velocity field data was obtained from either ADV measurements by the U.S. Army Corp of Engineers in a 1:40 scale forebay physical model, figure 3.1, or through actual field measurements collected during the summer of 1997. For the 1998 near field model, each inflow plane consisted of 12 three-dimensional physical model velocity points which were interpolated using a 0^{th} order scheme across the remaining surface region, i.e. the boundary velocities in the numerical model at a given point are assigned the same value as the nearest physical model data point. This same interpolation technique was adopted with actual field data measurements for use in the 1999 far-field model. Inlet conditions applied to both the 1999 modified near-field model and the 1999 super near-field model utilized the layered modeling approach and were extracted from their respective larger model, i.e. the inlet conditions used in the 1999 modified near-field model was generated from the solution of the 1999 far-field model.

3.3. Convergence Requirements

Owing, in some cases, to sizable cell skewness ratios of the computational domain, the convergence rate for the reduction of magnitude of residual errors was expected to be reasonably slow. In the present study, the following criteria were adopted to judge whether the numerical results were fully converged:

Reduction in magnitude of normalized residual errors, which are simply defined as the pseudo-time rate of change of a variable, by at minimum of three orders of magnitude for all of the following parameters:

(i) Pressure

(i) X, Y and Z velocity components

(ii) Turbulent kinetic energy and dissipation

(iii) Continuity

A typical convergence history is shown in figure 3.2. Nominal convergence times on the order of 10 hours were encountered using four processors on IIHR's SGI Powerchallenge Array depending on machine loading. Latter simulations were run on an Intel 550 Mhz Pentium III machine with nominal convergence times approximately equivalent to the SGI Powerchallenge Array.

3.4. Model Calibration and Validation

Having addressed a variety of important and relevant numerical issues in the previous sections, attention is now directed towards model calibration and validation. The following section reviews the initial 1998 near-field model calibration and validation followed by a discussion of the 1999 far-field model calibration and cross-validation of all 1999 models.

3.4.1. 1998 Near-Field Model Calibration

Calibration of the 1998 near-field model was completed using velocity data (Appendix B) obtained from the WES 1:40 scale physical model, figure 3.1, under 1997 flow and geometric conditions. The locations at which the calibration data were collected are presented in Appendix B. The procedure for calibrating a numerical model is similar to calibrating a physical model in which variables such as geometric grid refinement, and inlet/exit boundary conditions are progressively adjusted to produce close agreement between the experimental data and the numerical results. Comparison of the predicted velocity vectors at two representative cross-

sections can be found in figures 3.3 and 3.4. Extended comparisons between predicted and experimental velocity profiles are presented in appendix B of this report. The agreement is quite good with only appreciable differences along the face of the SBC at elevation 723.

To further justify the predicted flow features, comparisons between local flow angles are also plotted in appendix B. Despite some variability, agreement was found to be very good. However, as seen in the comparison of velocity magnitudes, inconsistencies are apparent near the water surface along the SBC gallery. Result from the numerical model show a small recirculation zone near the northern most SBC entrance. This feature is not, however, present in the experimental data. A qualitative explanation for this feature can be retrieved from the limited field data utilized along the inlet boundary plane. It will be shown in the 1999 cross-validation that imposing a more comprehensive inflow boundary condition data set can eliminate this feature.

During the calibration process, powerhouse discharges were computed to be significantly different then those reported with the physical model data. Nearest point, 0^{th} order interpolation of the 1997 inflow physical model data set to the inlet boundary domains yielded turbine discharges of 16.5 kcfs compared to the reported turbine settings of 19.8 kcfs in the physical model. Independent calculations based on average experimental velocities through each boundary plane and cross-sectional areas, however, resulted in turbine discharges of approximately 16.5 kcfs. Therefore, we believe the numerical model performed accurately and the reported 19.8 kcfs discharge was in error. These boundary conditions were subsequently scaled uniformly in all directions to produce the desired powerhouse discharges depending on SBC and powerhouse loadings.

3.4.2. 1998 Near-Field Model Validation

After satisfactory calibration, the numerical model was validated using two flow conditions generated in the 1:40 scale physical model using both the 1997 and 1998 geometry. It is assumed during the validation, that the inclusion, omission or change in the simulated Wells model insert (SWI) and local SBC geometric modifications will not affect the overall solution quality. Furthermore, adjustment made to the SBC operational settings are also assumed to have little or no significant affect to the solution integrity with only slight differences expected near the SBC entrances resulting from the altered SBC boundary conditions. Table 3.1 lists the calibration flow conditions as well as the two validation flow regimes. Appendix B presents the results of the validation through vector overlays.

Run #	Description	Powerhouse Discharge (kcfs)			SBC Discharge (cfs)			
		Unit 4	Unit 5	Unit 6	BGS	South	Middle	North
1	Original 1997 Geometry Used for **Calibration**	19.8	19.8	19.8	Closed	Closed	Closed	Closed
8	1997 SBC Geometry **Validation** Data Set #1	19.8	19.8	19.8	Closed	MAX 782	MAX 1272	MAX 1046
9	1998 SBC Geometry - BGS Installed WES **Validation** Data Set #2	19.8	19.8	19.8	MAX 817	MAX 1051	MAX 2132	Closed

Table 3.1 List of all test cases completed during the model calibration and validation.

The majority of the general flow features were replicated reasonably well under each validation case. Again, as in the calibration, a recirculation vortex was computed near the north SBC entrance. This feature was subsequently shifted towards the middle entrance when the surface collector operation changed and the north entrance was closed. As stated in the previous

section, this feature was eliminated during 1999 tests on account of applying a smooth more comprehensive inlet velocity profile.

3.4.3. 1999 Far-Field Model Calibration

Analogous to section 3.4.1, model calibration was also performed for the 1999 far-field model, however, actual field measurements were utilized for comparison rather than physical model data which was not available. No detailed comparisons were performed during this calibration process on account of limited availability of far-field data sets. The actual calibration was performed visually by comparing the general flow patterns using vector plots provided by engineers from the Walla Walla district of the US Army Corps of Engineers.

Results from the far-field calibration were relatively good with minimal disagreement in the near-field forebay area. Agreement was found to be inferior, however, along the southern riverbank approximately 3500 feet upstream. As discussed in section 2, these errors can be ascribed to simplification made during the grid generation process. Actual prototype geometry includes a small bay along the southern shoreline, however, this features is entirely disregarded in the numerical grid. This resulted in a single large vortex along the southern riverbank in the numerical model rather than two distinct recirculation regions in the prototype. Small secondary differences are also apparent in the vicinity of the lock and spillway and are most likely caused by geometric simplifications in that area.

3.4.4. 1999 Cross Validation

To ensure the accurate solution of the 1999 modified near-field model and the 1999 super near-field model, a cross validation was performed between each model and it's respective superior grid. Comparisons using equivalent bathymetric and geometric conditions together with matching operational loadings were completed in order to verify the accuracy of all 1999 grids.

It is notably evident that each model produces quite similar results with only general disagreement apparent near the entrance of the powerhouse intakes. The disparity in velocity contour in this region can be justified through examining the manner by which the exit boundary conditions are applied. In the 1999 far-field model, the numerical domain terminates at the face of the dam, consequently a perpendicular uniform velocity profile is assigned to each powerhouse intake at the dam face. In contrast, the 1999 modified near-field model extends approximately 50 feet into the powerhouse where an equivalent perpendicular uniform velocity profile is enforced. Without the inclusion of the powerhouse intake geometry and the subsequent translation of the uniform perpendicular velocity profile, an accurate representation of the true curving flow pattern cannot be attained.

Evidence of a second region where results differ is visible near the surface collection entrance weirs. These differences can again be explained, as in the above paragraph, through the different method of applying boundary conditions. The upstream face of the surface bypass and collection gallery where the exit boundary conditions are applied bound the 1999 far-field model. Conversely, the 1999 modified near-field model extends into the SBC gallery and allows for the boundary condition specification to be dramatically extended away from the entrance weir.

All remaining minor discrepancies apparent in the cross-validation are most likely due to slight differences in the dam or bathymetric geometry or variability in grid resolution. This issue of studying changes in grid resolution is entitled grid dependence and can be investigated through the use of three separate grid densities under equivalent boundary conditions. Ideally, the grid utilized for this study would produce the same results as a grid of twice the density. No rigorous grid dependence study was performed due to the lack of the required computing resources and

required time and financial effort, however the results would have undoubtedly helped to better address CFD error associated with the current Lower Granite Dam application.

Figures 3.5 and 3.6 characterize the cross-validation completed between the 1999 modified near-field model and the 1999 super near-field model. Results showed quite good agreement between the models with only minor differences present near the surface collection gallery intake. The differences can best be explained through the ability of the super near-field model to better resolve some of the structural geometry due to its high grid densities.

3.5. Summary

Section 3 presented some general details of the numerical model as well as the boundary conditions applied. This was followed by a description of the convergence requirements enforced. Calibration and validation of both the original 1998 near-field model and all three 1999 models concluded the section. The following section will focus on presenting the results from a majority of the test scenarios. This will be followed by a detailed narration of the process undertaken to design the super-BGS intake configuration. Concluding this section is a detailed description of the final super-BGS surface collection entrance characteristics and design.

4. RESULTS

This section chronologically illustrates the general test scenarios and discusses their intent and outcome. This discussion culminates in a comprehensive description of the final super-BGS entrance design that will be installed on the prototype for testing prior to the summer of 2000.

4.1. 1998 Near-Field Model

A total of fifteen simulations corresponding to the 1998 near-field model were undertaken. Table 4.1 lists each modification studied along with its respective flow condition and geometric design. For presentation clarity, the changes to the fish diversion structures will be sub-classified into geometric changes, whereby modifications to the actual structure have been examined, and operational changes, where adjustment to the SBC operation as well as powerhouse discharges were varied.

4.1.1. Geometric Modifications

Four separate geometric modifications were examined under the 1998 geometric conditions and are listed in Table 4.1. Modifications 1 and 2 involved alterations to the underside of the 1998 surface bypass and collection (SBC) configuration. Modification 3, the Simulated Wells model Insert (SWI), attempted to apply a proven design from Wells Dam (Douglas County, PUD) to the powerhouse intake geometry as well as the underside of the SBC. The final alteration, modification 4, constituted the installation of the Behavioral Guidance Structure (BGS) curtain. Each scenario required a separate numerical grid but utilized the same upstream and downstream boundary conditions, thus allowing for easy comparison. Additionally, a fifth grid (Run#2) was established with no geometric modifications to be utilized as a baseline for all comparisons.

Modification 1 (Run#4) consisted of the addition of a well-rounded extension fillet placed along the underside of the 1998 SBC collection system, figure 5.1. This enhancement provided smoothing to the velocity field directly beneath the SBC as well as a slight reduction in the overall turbulence levels in its vicinity. There was not, however, any detectable affect to the flow entering the surface collection facilities.

Modification 2 (Run#5) was composed of a 30-ft radius lip extension added to the bottom corner of the upstream face of each SBC unit, figure 4.2. This alteration produced a large stagnation region just above the lip extension. The extension also produced a large velocity gradient as the flow passed around the lip and entered the powerhouse. Subsequently, this caused higher velocities and turbulence levels slightly upstream compared with modification 1, yet little affect on overall velocity magnitude and direction in the vicinity of the surface collection weir was evident.

The third structural modification studied (Run#3) was the simulated wells model insert (SWI) design. The design changes can best be characterized by reproducing the Wells Dam intake geometry in Lower Granite's intake bays, figure 4.3. Results from this change produce significant alterations to the flow field directly beneath the surface collection gallery and extending to the rear of the intake bay. The insert was also able to further smooth the velocity gradients and turbulent energies as the flow entered the intake bays, however as with the results from the previous two modifications, little or no affect on the SBC entrance conditions were evident.

The fourth and final geometric modification was the inclusion of the behavioral guidance structure (BGS) curtain. Because the 1998 model only extends southeast to the start of powerhouse unit 4 and upstream 200 feet, only about 20 percent of the BGS was included along

the southern most boundary. No significant variations to the surface collector flow patterns were apparent along the vertical plane. Beginning about 100 feet upstream from the surface collection entrances, however, the general flow direction shifted northward due to the BGS curtain presence. This, consequently, induces the formation of several gradual vortices along the surface collector face, which were not predicted when excluding the BGS. Figure 4.4 illustrates this shift of the flow pattern when the BGS is installed.

4.1.2. Operational Modifications

Table 4.1 lists all major operational modifications tested using the 1998 model. Because each operational modification incorporated a variety of the geometries presented in section 4.1.1, identification of all local hydrodynamic effects unique to each operational change is quite difficult. To facilitate understanding these variations, purely general conclusions will be discussed focusing solely on the operational affects.

The first operational scenario (Run#9) examined the flow characteristics in front of the surface collection gallery under the maximum powerhouse operational conditions of 118.8 kcfs (19.8 kcfs per turbine). This flow will be considered a baseline condition against which the following two types of operational changes will be compared.

Simulation of the minimum powerhouse flow condition was the second operational flow case studied and focused solely on extreme powerhouse loading events. The minimum operational discharge through the powerhouse is 93 kcfs (15.5 kcfs per turbine). When comparing this to the maximum flow conditions, a significant overall variation in total velocity magnitude is present. As expected, the 20% decrease in powerhouse discharge generally resulted in a proportional decrease in velocity magnitude under low powerhouse conditions. This trend was also mirrored in total acceleration and turbulence levels, which exhibited a similar uniform,

decrease for both hydraulic characteristics under low flow conditions. Furthermore, little to no change in local flow direction is visible throughout the entire domain.

The remaining operational modification involved varying the overall area of the SBC entrances. This was accomplished by altering the entrance weir position vertically to achieve the desired discharge. One specific entrance configuration fixed the opening depths equivalently to a successful configuration utilized at Ice Harbor Dam, which is located downstream from Lower Granite on the Snake River. The aim for this design test was to attempt to reproduce flow patterns similar to those present in the forebay of Ice Harbor Dam. As in all of the previous 1998 simulations, no uniquely different hydrodynamic field was computed using this new configuration. This strongly supported the general hypothesis that forebay hydrodynamics are site specific and minor geometric or operational changes would results in little or no global enhancement to the forebay hydraulics. Appendix C provides representative illustration of the 1998 simulation results.

One particular area of interest with regard to surface collector design is the zone of capture. This zone is defined as the region of water that enters the surface bypass gallery. Functionally, this zone can be computed by tracking three-dimensionally the velocity gradients upstream from a continuous boundary characterizing the surface collection intake opening. For illustration purposes, figure 5.5 depicts the zone of capture for both 1998 and 1999 flow and geometric conditions.

Altogether, each 1998 geometric and operational configuration produced quite equivalent zone of capture regions. This was generally expected because each case used equivalent SBC discharge settings. It will be shown in the following sections that moderate changes can be achieved with respect to zone of capture by significantly increasing the SBC discharge.

4.2. 1999 Far-Field Model

Initial tests completed using the 1999 geometric and flow conditions incorporated the entire river width and dam geometry extending upstream approximately one mile. A more detailed description of the grid topology utilized can be found in Section 2 of this report. Two particular flow conditions, high and lower powerhouse settings, were initially examined using the 1999 far-field model. For both of these cases, the BGS curtain was not deployed.

Results between both initial 1999 far-field test cases showed little change in the general flow pattern. As expected, a proportional reduction in the overall velocity magnitude was apparent in the lower powerhouse case, however no other dominant variations were visible.

To allow for the inclusion of the BGS curtain in any subsequent simulations, its addition and the recalculation of the above test cases would be required to produce an accurate set of boundary conditions to be used in the finer scale near-field and super near-field models. Consequently, the previous two test cases were run a second time with the inclusion of the full BGS curtain.

Results exhibit similar flow patterns throughout the extent of the model except in the vicinity of the BGS curtain. A substantial acceleration and subsequent increase in both velocity and turbulence is apparent in the contraction caused by the convergence of the BGS and shoreline. Further downstream and adjacent to the BGS curtain, a large upwelling current is also exhibited due to the flow abruptly curving up as it passes under the curtain, figure 4.6. Along the face of the dam, the general flow pattern just to the north of the BGS curtain indicates a substantial amount of water enters the BGS surface collection entrance from the south. This feature is not evident when the BGS is removed.

As discussed earlier, the man reason for constructing the far-field model was to generate accurate boundary conditions for the more geometrically precise near and super near-field grids. In actuality, the 1999 far-field model was constructed for three additional proposes intended for future study. The numerical fish surrogate algorithm developed by Nestler et. al. will be applied to the entire forebay region in an attempt to better understand and predict fish behavior beyond the near-field forebay region. Through statistical regression between CFD results and sequential fish position data, new information can be attained correlating fish response to hydraulic phenomena. The second application of the 1999 far-field model results will focus on examining the flow patterns in the vicinity of the contraction produced by the convergence of the behavior guidance curtain and the southern shoreline. The final function of the 1999 far-field model will be to provide a more comprehensive data set for a larger scale calibration study using turbulence and acceleration quantities in addition to velocity vectors. Presently, ongoing data collection and quality assurance are being completed on the measured ADV (Acoustic Doppler Velocimeter) data sets for this future application.

4.3. 1999 Modified Near-Field Model

During the fall and winter months of 1998 and 1999, the Corps performed a detailed fish count in the vicinity of the SBC gallery at Lower Granite Dam. This study indicated that the BGS and middle entrances collected the majority of the juvenile fish. Accompanied by these statistics, it was decided to focus the numerical modeling efforts towards examining modifications to these two particular entrances. Because of the proximity of the behavior guidance curtain to the BGS surface collection entrance, focus was further refined to that area

where the possibilities of more enhancements to the flow field were available. Table 4.2 illustrates each trial performed during the 1999 testing period.

Four separate studies, C1 through C4, were undertaken using the 1999 modified near-field model without the presence of the BGS curtain. Runs C1 and C2 utilized the same grid and boundary conditions with one exception. Run C1 withdrew 2000 cfs at both the middle and BGS surface collection entrances, while run C2 withdrew 4000 cfs from the middle entrance alone. The powerhouse discharge for both cases was set to the maximum allowable loading corresponding to 19,800 cfs per turbine unit or a total of 118,800 cfs. The entire facility loading, including the powerhouse, spillways and surface collection intakes, was set to 170,300 cfs for both cases.

Runs C3 and C4 were geometrically and operationally similar to C1 and C2 respectively with one minor difference. For both cases, the powerhouse loading was reduced from 19,800 cfs to 15,500 cfs for powerhouse units 4 – 6. This effectively reduced the overall plant loading from 170,300 cfs to 150,500 cfs. All remaining operational conditions were held constant between each condition.

Results from cases C1 and C3 show almost identical flow patterns in the vicinity of the surface collection entrances. Runs C2 and C4 also reproduce comparable velocity fields in the surface collector region. Appendix D includes general contour plots from all the 1999 modified near-field model simulations. Inspection of the flow patterns further upstream show slight deviations in total velocity magnitude, however the local flow direction remains constant. These general trends were anticipated on account of the utilization of similar scaled upstream boundary conditions.

One final test was performed using the 1999 modified near-field model, run C5. This test case was similar to run C3, however the BGS curtain was deployed and the middle SBC entrance weir was lowered 11 feet. Results from this test again showed quite similar flow patterns in the vicinity of the middle SBC entrance, however the overall velocity magnitude decreased slightly due to deeper intake configuration. The local approach angle directly south of the BGS entrance, however, was shifted by the curtain presence and forced the majority of the flow into the BGS entrance from the south, figure 4.7.

A comparison was completed between the 1998 and 1999 near-field model zone of capture to illustrate all enhancements achieved during this period. Generally under 1999 operational and geometric conditions, the vertical extent of the zone of capture increased, figure 4.5. This feature exhibits the potential capability of attracting juvenile fish from a greater portion of the water column.

As the zone of interest began to focus on a more refined region in and around the BGS and middle SBC intakes, it was determined that a finer grid was required. This new mesh, the 1999 super near-field model, intended to achieve higher solution quality by capturing more geometric detail in the SBC entrance gallery. Thus began simulations with the 1999 super near-field model.

4.4. 1999 Super Near-Field Model

Four successive alterations to the prototype BGS opening configuration were studied using the 1999 super near-field model. Each successive modification evolved through enhancements of the interior SBC shape by adding a number of smooth transitions, fillets, geometric changes, and shaped structural piers. The following four sections will briefly describe each successive modification concluding with a detailed description of the final BGS entrance

shape. The general goals for each new entrance design intend to minimize both turbulent kinetic energy and vertical acceleration gradient while providing a smooth velocity field throughout the intake gallery region.

4.4.1. Entrance Design #1

The initial configuration for the proposed super-BGS entrance is discussed below. The design includes two separate opening slots bisected by a vertical structural member with a total effective area of 210.0 square feet. A constant vertical 1:2 slope was adopted for the floor of the intake striving to achieve a smooth velocity field as the water enters the gallery. Immediately following the sloping intake base, a false floor extends to the opposite wall thus maintaining the overall intake depth. This false floor further extends downstream approximately 20 feet where it abruptly joins the full SBC gallery depth thus inducing a large vertical recirculation as the flow passes over the backward facing step. Below the surface floatation box, the back 90° corner of the intake was replaced with a constant 9-foot radius curve. The region between the surface floatation box, which extends vertically down from the water surface approximately 6 feet and provides floatation for the entire SBC gallery, remained unchanged. In addition, no smooth geometric shaping was applied to any structural members.

The resulting hydrodynamic characteristics predicted for entrance design #1 will be considered a baseline for all subsequent tests. Results for case exhibit a generally smooth velocity field immediately upstream from the intake. Directly to the rear of the vertical structural member bisecting the inlet, a stagnation region is exhibited. In addition, high levels of turbulent kinetic energy were also predicted in this vicinity, figure 4.8. On a local scale, the calculated flow field illustrates notably high levels of total velocity along the back wall of the gallery exposing the need to adjust the back wall radius to ensure a smoother flow transition around the

interior of the SBC gallery. Focusing more on the vertical acceleration gradient and turbulent kinetic energy, it is apparent that the elimination of any abrupt geometric changes will presumably reduce these quantities throughout the domain. These concepts were then adopted for the second test iteration.

4.4.2. Entrance Design #2

The second design configuration attempted to eliminate the locally high turbulent levels resulting from the linear intake geometry by adding smooth curves between all slope transitions. In addition, in order to increase the total velocity magnitude, the side-walls of the entrance formed a linear contraction with both walls slanting inward at a rate of 4.5:1. Immediately beyond the side-wall contraction and smooth sloping intake, the false floor was lowered 5 feet in an attempt to conserve global continuity and thus reduce overall accelerations. Finally, the 9-foot back corner radius was replaced with a straight wall at a 30° angle from the back wall to try to ensure further smoothing as the flow passed around the bend. The concept was also applied to the region between the upper floatation box and the water surface.

These improvements moderately decreased the overall turbulent kinetic energy levels directly behind the intake separation members, however increased turbulence levels are apparent further inside the gallery. This growth in turbulent energy is due to the increased angle through which the flow must curve more dramatically around as a result of the side-wall contraction, figure 4.9. When examining the additional smooth geometric transitions and fillets, it can be seen that due to limitations on grid density, the curve is actually modeled as a number of short straight lines, thus resulting in discrete slope changes and slightly higher then expected levels of turbulence. A reduction in turbulence in these regions, however, was apparent when compared to the previous case. Concentrating on the region where the false floor was lowered 5 feet, high

levels of vertical acceleration are evident. The concept of conserving mass on a global scale works well, however, locally strong acceleration gradients are present consequently increasing undesirable hydraulic characteristics. While this design exhibited modest results in eliminating local turbulence, it revealed no apparent enhancements to the high vertical acceleration gradients present inside the SBC gallery. The ensuing design iteration attempts to address these issues with new large scale geometric smoothing.

4.4.3. Entrance Design #3

The third refinement to the BGS intake made an effort to eliminate the large vertical acceleration gradients caused by any abrupt geometric change. Furthermore, this design will seek to reduce all remaining regions of high turbulence through extensive small scale geometric smoothing. The proposed modification combined the knowledge from the previous attempts into a single smooth transition linking the entrance weir to the main gallery channel. This was accomplished by linearly interpolating between all boundary cross-sections to form a highly complex, truly smooth floor transition.

Results showed reasonable improvements with respect to both turbulent kinetic energy and vertical acceleration, reducing their levels significantly yet expanding the overall spatial variability, figure 4.10. Further complications concerning this configuration revolved around the highly complex interior shape resulting from the linear interpolation. It was decided that one final design would be tested of which contained many of the successful characteristics displayed in the three previous simulations yet contained a more simplified geometry.

4.4.4. Entrance Design #4

The forth and final design iteration for the super-BGS intake configuration combined the ideas derived from the previous trials with the addition of some basic constructability

improvements. Figure 4.11 shows the design drawings completed for 2000 prototype construction and includes the following features:

(i) 4:1 side-wall contractions extending 12-feet into the SBC gallery;

(ii) 1:2 bottom slope extending 10-feet into the intake and merging with a 5-foot; radius curve ending vertically a total of 12-feet into the gallery;

(iii) Smoothly shaped separation member with 4-foot radius bevel curve;

(iv) 15-foot radius back-wall curve extending vertically to the base of the float (elevation 728-feet);

(v) 12-foot radius back-wall curve extending from the base of the float to the water surface;

(vi) 10-foot radius extending northward into the SBC gallery to the upstream gallery wall; and

(vii) Removal of floatation box in front of BGS entrance.

Results from the final design configuration (C1-D) illustrate an overall reduction in both the turbulence levels and vertical acceleration gradient throughout the intake region. The enhancements also greatly diminish the spatial flow variability by providing moderately smooth transitions throughout. Figure 4.12 illustrates predicted levels of both vertical acceleration and turbulent kinetic energy for the final 1999 super-BGS entrance design. Results from actual prototype testing have not been completed as of the conclusion of this research, however the final numerical simulations show encouraging hydrodynamic features.

4.5. Summary

General results attained during 1998 testing failed to provide any uniquely different hydrodynamic flow fields. With the additional benefits contained in the layered modeling

approach and the accompanying biological fish count data, the 1999 runs focused their efforts on the shape and discharge of the BGS intake. Results from the 1999 far-field model produced a comprehensive set of boundary conditions for the 1999 modified near-field model, which illustrated potential design configurations, and operational loading for the BGS entrance. Due to limited grid densities and extended convergence times, however, a super near-field model was adopted. The 1999 super near-field model was applied iteratively to the BGS intake ultimately achieving an optimal design, which minimized turbulence and vertical acceleration while producing a generally smooth velocity field throughout. This design will be constructed for 2000 prototype testing. In addition, the super near-field model emphasized the capabilities of CFD as a design tool in surface bypass and collection situations.

Run #	Description	Powerhouse Discharge (kcfs)			SBC Discharge (cfs)			
		Unit 4	Unit 5	Unit 6	BGS	South	Middle	North
1	Original 1997 Geometry Used for Calibration	19.8	19.8	19.8	Closed	Closed	Closed	Closed
2	1998 SBC Configuration BGS Installed	19.8	19.8	19.8	Closed	Closed	Closed	Closed
3	1998 Simulated Wells Model Insert (SWI) BGS Installed	19.8	19.8	19.8	Closed	Closed	Closed	Closed
4	1998 SBC Geometry - Modification #1 Well Rounded Fillet	19.8	19.8	19.8	Closed	Closed	Closed	Closed
5	1998 SBC Geometry - Modification #2 35' Lip Extension	19.8	19.8	19.8	Closed	Closed	Closed	Closed
6	Enhanced Wells Model Insert BGS Installed - Deep SBC Entrances	19.8	19.8	19.8	MAX 2000	Closed	MAX 2000	Closed
8	1997 SBC Geometry Validation Data Set #1	19.8	19.8	19.8	Closed	MAX 782	MAX 1272	MAX 1046
9	1998 SBC Geometry - BGS Installed WES Validation Data Set #2	19.8	19.8	19.8	MAX 817	MAX 1051	MAX 2132	Closed
11	1998 SBC Geometry - BGS Installed Low Powerhouse Flow - 15.5 kcfs	15.5	15.5	15.5	MAX 817	MAX 1051	MAX 2132	Closed
12	1998 SBC Geometry - BGS Installed Ice Harbor SBC Configuration - High Flow	19.8	19.8	19.8	IHR 1719	IHR 570	IHR 918	IHR 793
13	1998 SBC Geometry - BGS Installed Ice Harbor SBC Configuration - High Flow	15.5	15.5	15.5	IHR 1719	IHR 570	IHR 918	IHR 793
14	1998 SBC Geometry - BGS Installed Operational Version #3	15.5	15.5	15.5	2000	Closed	2000	Closed
15	1998 SBC Geometry - BGS Installed Operational Version #1	15.5	15.5	15.5	MAX 1599	Closed	MAX 2411	Closed
16	1998 SBC Geometry - BGS Installed Operational Version #2	15.5	15.5	15.5	3000	Closed	Closed	Closed
17	1998 SBC Geometry - BGS Installed Operational Version #4	15.5	15.5	15.5	Closed	Closed	4000	Closed

Table 4.1 Comprehensive list of 1998 test conditions.

Run #	Description	Operational Loadings		SBC Discharge (cfs)			
		Total Loading (cfs)	Powerhouse Loading (cfs)	BGS	South	Middle	North
F1	1999 Far-Field Model Full Powerhouse - NO BGS	170,300	118,800	Closed	Closed	Closed	Closed
F2	1999 Far-Field Model Low Powerhouse - No BGS	150,500	118,800	Closed	Closed	Closed	Closed
F3	1999 Far-Field Model Full Powerhouse - BGS Installed	170,300	93,000	Closed	Closed	Closed	Closed
F4	1999 Far-Field Model Low Powerhouse - BGS Installed	150,500	93,000	Closed	Closed	Closed	Closed
C1	1999 Modified Near-Field Model SBC Operational Configureation - C1	170,300	118,800	MAX 2000	Closed	MAX 2000	Closed
C2	1999 Modified Near-Field Model SBC Operational Configureation - C2	170,300	118,800	Closed	Closed	MAX 4000	Closed
C3	1999 Modified Near-Field Model SBC Operational Configureation - C3	150,500	118,800	MAX 2000	Closed	MAX 2000	Closed
C4	1999 Modified Near-Field Model SBC Operational Configureation - C4	150,500	118,800	Closed	Closed	MAX 4000	Closed
C5	1999 Modified Near-Field Model Same as C2 with BGS Deployed	170,300	118,800	MAX 2000	Closed	MAX 2000	Closed
C1-A	1999 Super Near-Field Model BGS Configuration #1	170,300	118,800	MAX 2000	Closed	MAX 2000	Closed
C1-B	1999 Super Near-Field Model BGS Configuration #2	170,300	118,800	MAX 2000	Closed	MAX 2000	Closed
C1-C	1999 Super Near-Field Model BGS Configuration #3	170,300	118,800	MAX 2000	Closed	MAX 2000	Closed
C1-D	1999 Super Near-Field Model BGS Configuration #4	170,300	118,800	MAX 2000	Closed	MAX 2000	Closed

Table 4.2 Comprehensive list of 1999 test conditions.

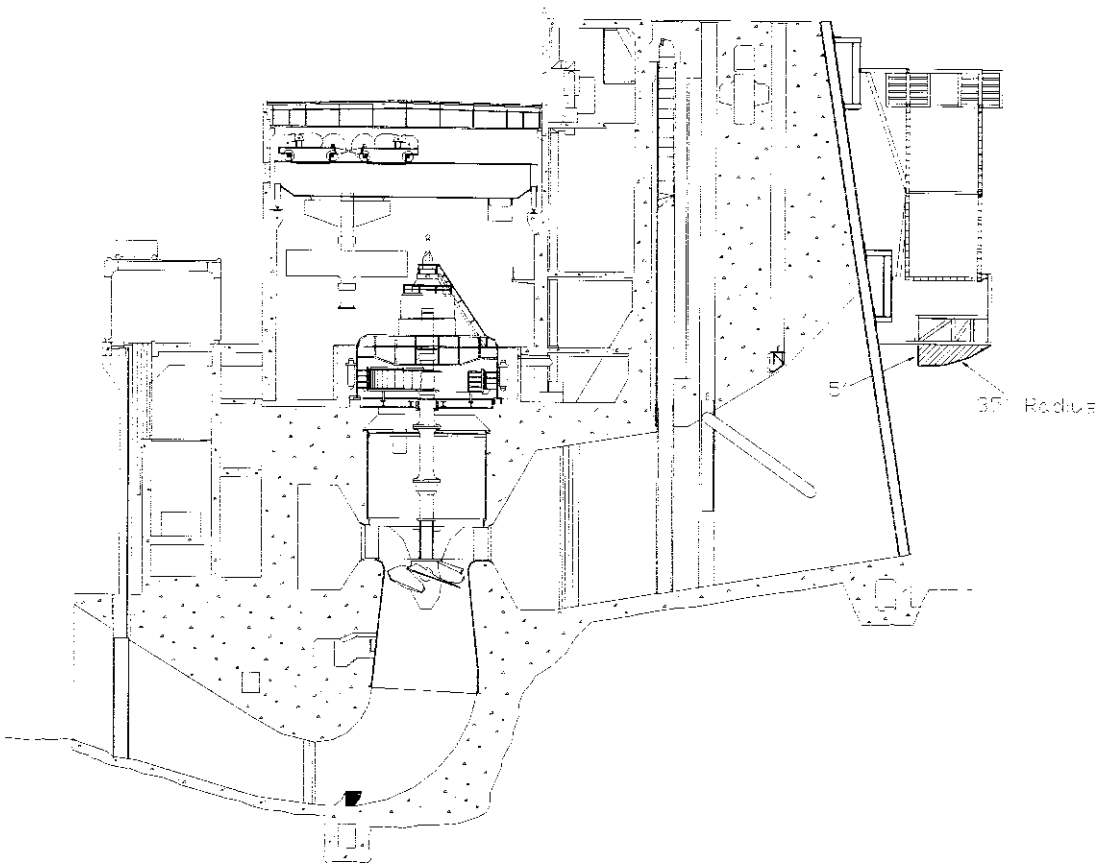

Figure 4.1 Elevation view of 1998 near-field model modification 1 with the 35 foot radius along the underside of the SBC gallery.

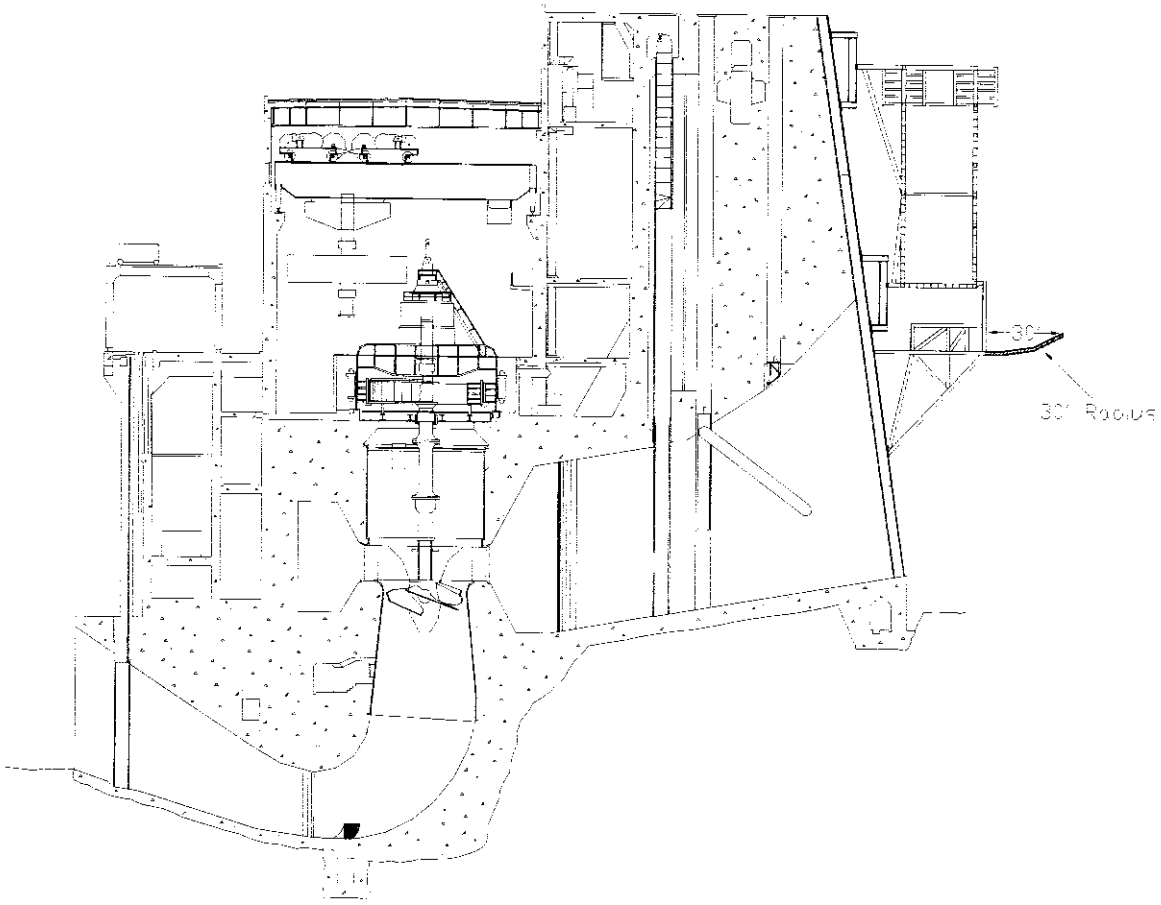

Figure 4.2 Elevation view of 1998 modified near-field model, modification 2, with the 30 foot radius extension lip.

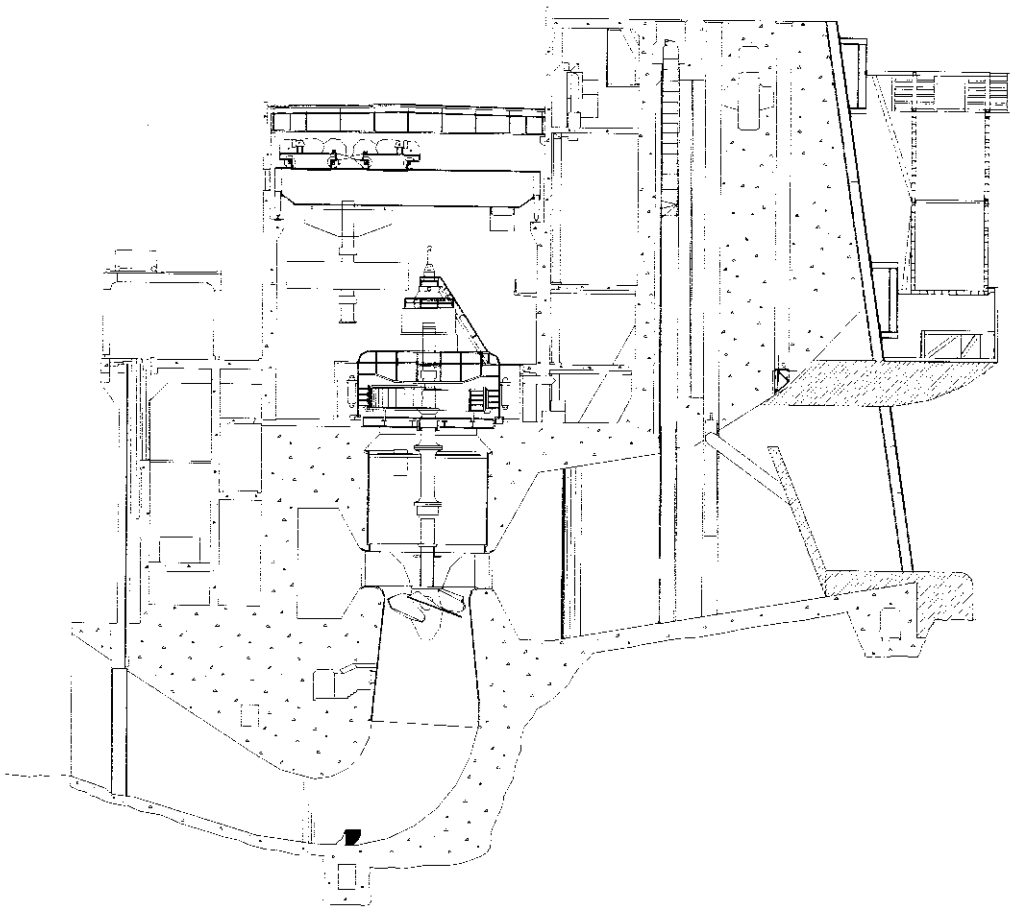

Figure 4.3 Elevation view of 1998 near-field model, modification 3, with the Simulated Wells Model Insert (SWI) installed.

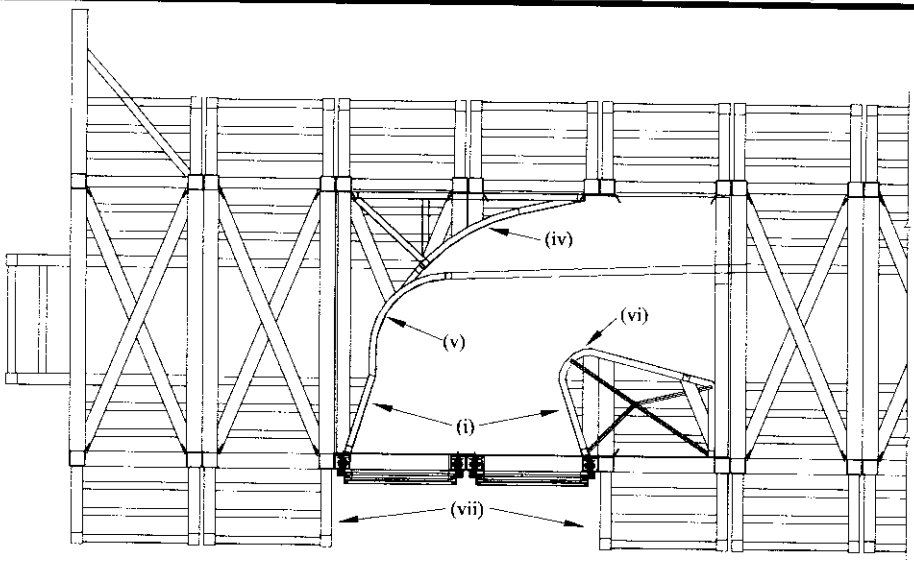

a) Top view

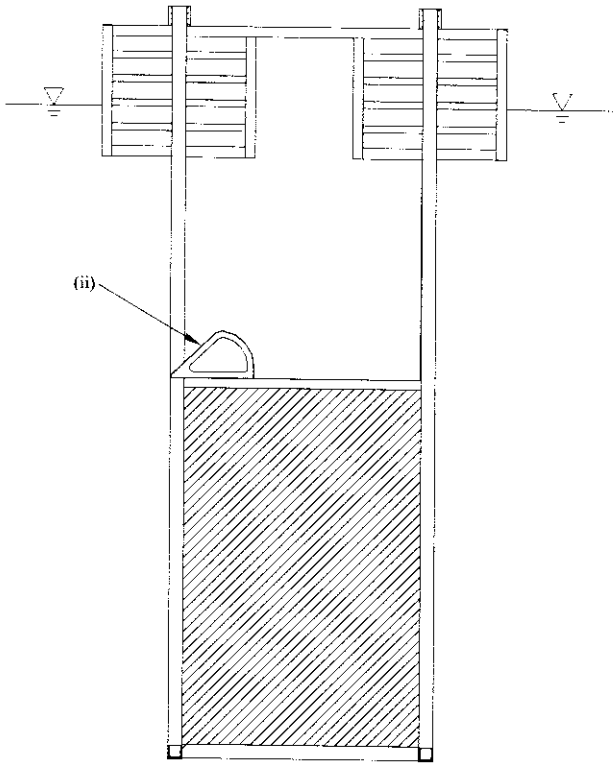

b) Side view

Figure 4.11 Final technical drawings for the 1999 Super-BGS entrance design.

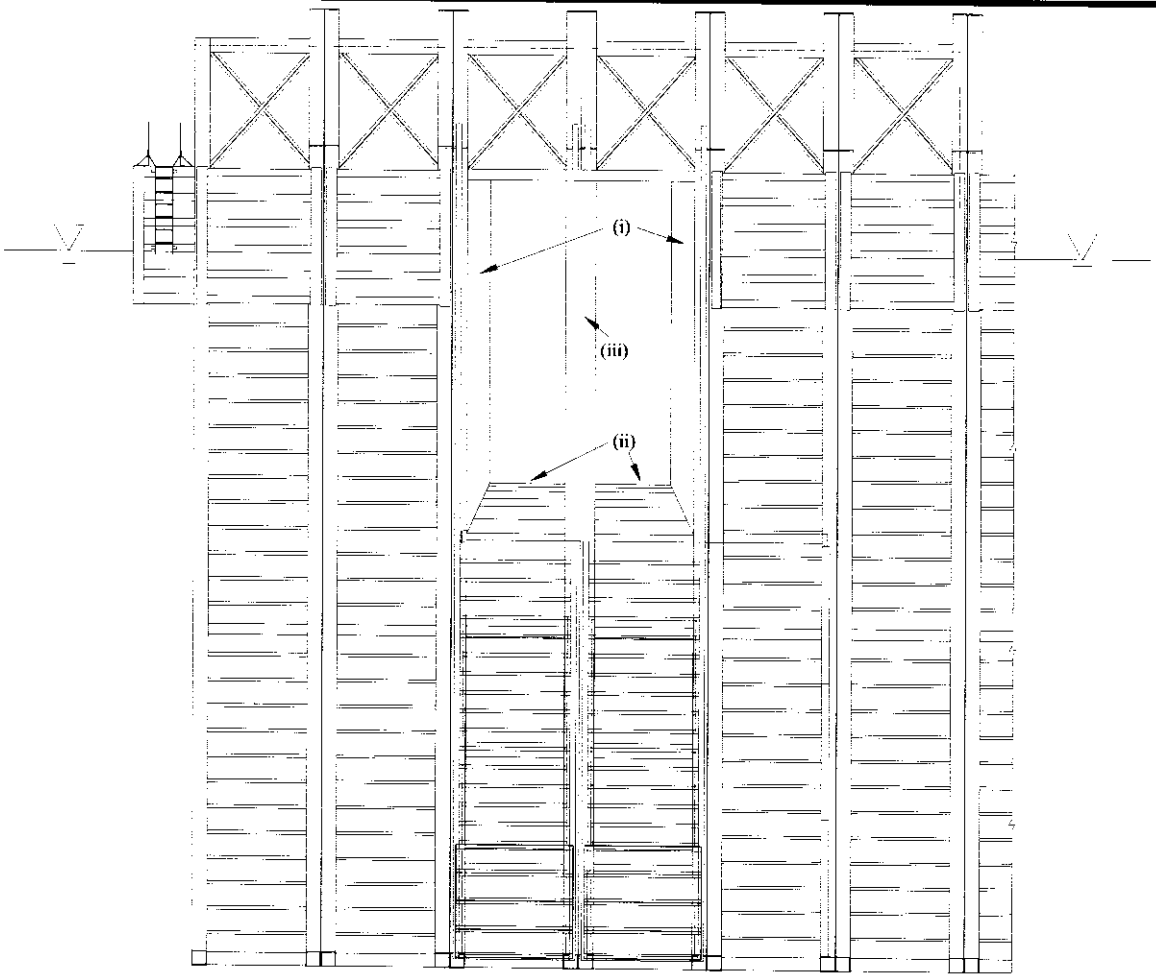

c) Front view

Figure 4.11 continued.

5. CONCLUSIONS

This study illustrates the application of computational fluid dynamics (CFD) modeling as a tool to aid in the design of fish passage facilities. The specific objectives of the study were to evaluate the current hydraulic conditions at Lower Granite Lock and Dam, and to test design feasibility, in addition to providing design enhancements and recommendations for future structural and operational modifications. Furthermore, this investigation has provided a set of detailed three-dimensional vector fields of the overall forebay region to be available for future research endeavors.

Results from this numerical model study were intended to address the following issues:

(i) show the dependence on detailed grids to ensure adequate solution accuracy;

(ii) present the ability to efficiently model many different flow scales using the layered modeling approach;

(iii) illustrate the ability to accurately capture the complex flow features found in a river/hydropower system;

(iv) show the capabilities of CFD as a design tool in fish passage; and

(v) optimize the design of the super-BGS surface collection intake to be constructed for 2000 testing.

The level to which the above objectives were accomplished are summarized in the following section:

(i) Solution dependence on detailed grid topographies

Throughout each stage of this study, it became evident that superior solution accuracy could be achieved through the incorporation of more complex geometric features. Initial tests, which utilized dramatic simplification to the river bed and dam shape, showed good agreement to experimental data on a global scale but deteriorated when more local flow features were examined. As the grid topology advanced, more detailed geometric features were included and overall agreement improved both globally and locally.

(ii) Layered Modeling Approach

The ability to capture largely varying flow scales in a river/hydropower system is crucial for solution accuracy. Ideally, a fine resolution grid would be adopted throughout the entire model domain, however solution efficiency is compromised. The layered modeling approach utilized in this study attempted to maintain both solution accuracy and efficiency through three successively finer resolution overlapping grids.

Initial tests competed under 1998 operational and geometric conditions illustrated the need to replace the single grid arrangement with a layer model through complications surrounding calibration and validation agreement. When similar operational and geometric conditions were computed using the layered modeling approach, excellent agreement was found in both calibration and cross-validation.

(iii) Accuracy of the numerical models in complex river/hydropower systems:

It was found that the ability of the numerical models utilized in this study to capture the complex flow physics present in and around Lower Granite Dam were generally accurate with respect to overall physical model and field data sets. The dominant flow characteristics including overall plant discharge and general recirculation zone size and location were visually in good agreement with the available data. On a more regional flow scale, local velocity magnitude and direction also reflected those features apparent in the experimental data. Those regions exhibiting reduced accuracy can generally be attributed to poor boundary conditions or inadequate grid resolution, however their error was not propagated throughout the remainder of the domain.

(iv) Capabilities of CFD as design tool in fish passage

Throughout the duration of this investigation, many design and operational enhancements were tested with varying levels of success. A total of 35 distinct geometric and operational scenarios were evaluated during the two-year study period. The predominate enhancements completed during this research focus on the Behavioral Guidance Structure (BGS), the surface collection intake shape, and the overall collection gallery configuration to name a few. When compared with costly, in both a time and economic sense, physical models and field studies, CFD provided the only realistic feasible solution. The research completed in this study has helped to advance the use of CFD in surface collector design and operation.

(v) Optimization of the super-BGS intake structure

Driven by the Corps' need to explore the flow characteristics and feasibility of possible year 2000 design modifications to the surface collection entrance, the numerical model was run iteratively to derive a final design shape for the super-BGS entrance. Beyond satisfying global discharge and velocity requirements, the final super-BGS design dramatically reduced overall flow gradients and turbulence thus demonstrating potential improvements in its fish attraction. The reader is directed to section 5.4.4 for a more rigorous description and figures of the final super-BGS intake design. Results from actual prototype testing have not been completed as of the conclusion of this research, however the final numerical simulations showed encouraging hydrodynamic features.

References

Amtec, (1996), "Tecplot User's Manual Version 7", Bellevue, WA.

Bell, M.C. and DeLacy, A.C., (1972), "A Compendium on the Survival of Fish Passing through Spillways and Conduits", Fisheries Engineering Research Program, U.S. Army Engineering Division, Contract # DACW57-67-C-0105, Portland, OR.

Blank, J.C., Weber, L.J., (1999),"Evolution of Numerical Simulations of Fish Passage Facilities at Lower Granite Lock and Dam", ASCE Water Resources Conference, August.

Christensen, P.J., Wielick, R.G., (1995), "Attraction Flow – A Fish Bypass Alternative", Technical Paper, ASCE Waterpower 95.

Farr, W.E., (1974), "Traveling Screens for Turbine Intakes of Hydroelectric Dams", Report No. 15 (Cooling Water Research Project), John Hopkins University, Baltimore, MD.

Fluent, (1997), "FLUENT/UNS & RAMPANT 4.2 User's Guide", Lebanon, NH.

Francfort. Et. al., (1994), "Environmental Mitigation at Hydroelectric Projects. Benefits and Costs of Fish Passage and Protection", US Department of Energy, Idaho Operations Office, pp. 19:1-19:17.

Gridgen, (1997), "Version 13 User Manual", Pointwise Inc, Fort Worth, TX.

Haug, P.J., (2000), "Wanapum Dam Spillway Deflectors," Master Thesis, The University of Iowa.

Huang, J., Weber, L.J., (1998), "Numerical Simulations of the Forebay of Lower Granite Lock and Dam.", Proceedings of the International Water Resources Conference, HydroVision 98, American Society of Civil Engineers, pp. 349-358.

Johnson, G.E., Giorgi, A.E., Erho, M.W., (1997), "Critical Assessment of Surface Flow Bypass Development in the Lower Columbia and Snake Rivers", US Army Corps of Engineers, Portland and Walla Walla Districts.

Krcma, R.F., Farr, W.E., and Long, C.W., (1980), "Research to Develop Bar Screens for Guiding Juvenile Salmonids Out of Turbine Intakes at Low Head Dams on the Columbia and Snake Rivers", National Oceanic and Atmospheric Administration National Marine Fisheries Service, Northwest and Alaska Fisheries Center, Seattle, WA.

Kurdera, E.A., Sullivan, C.M., (1993), "Evaluation of the Smolt Bypass System at Wells Dam in 1992" Final Report. BioSonics, Inc., Seattle, Washigton.

Lai, Y.G., (1999), "An Unstructured Grid Arbitrarily Shaped Element Method for Fluid Flow Simulations", AIAA-99-3711, 30th AIAA Fluid Dynamics Conference, Norfolk VA.

Lai, Y.G. and Patel, V.C., (1999), "CFD Simulation and Assessment of the Draft Tube Flow", Turbine-99, ERCOFTAC Workshop on Draft Tube Flow, Porjus, 29 Sweden.

Meselhe, E.A., Odgaard, A.J., (1998), "3D Numerical Flow Model for Fish Diversion Studies at Wanapum Dam", Journal of Hydraulic Engineering, December 1998, pp 1203-1214.

Meselhe, E.A., Weber, L.J., Odgaard, A.J., Johnson, T., (2000), "Numerical Modeling for Fish Diversion Studies.", IIHR Technidcal Report (in prepatation), University of Iowa.

National Marine Fisheries Service, (1995), "Proposed Recovery Plan for Snake River Salmon", National Marine and Fisheries Service, March.

Nestler, J.M., (2000), "Development of a Numerical Fish Surrogate for Improved Selection of Fish Passage Design and Operation Alternative for Lower Granite Dam: Phase I", Technical Report, US Army Corps of Engineers.

Nielson, K.D., Weber, L.J., Bennion, D.K., (1998) "Design Challenges of the Lower Granite Dam Behavioral Guidance Structure for Guiding Migrating Fish in the Powerhouse Forebay", Proceedings of the International Water Resources Conference, HydroVision 98, American Society of Civil Engineers, pp. 349-358.

Normandeau Associates, Inc., Parametric, Inc, and Skalski, J.R., (1996), "Behavior of Juvenile Salmonids Relative to the Surface Bypass and Collection Channel at Wanapum Dam, Columbia River, Washington", Prepared for Grant County Public Utility District No. 2, Ephrata, WA.

Odeh, M., Haro, A., Norieka, J., (1997), "Evaluation of a Uniform Acceleration Weir for Downstream Bypass Entrances" Fish Passage Workshop, Milwaukee, WI.

Odgaard, A.J., Cherian, M.P., and Elder, R.A., (1987), "Fish Diversion in Hydropower Intake", Journal of Hydraulic Engineering, ASCE, Vol. 113, No. 4, pp505-519.

Peven, C.M., (1998), "Development of a Juvenile Salmon Bypass System at Rocky Reach Dam, Columbia River", Proceedings of the International Water Resources Conference, HydroVision 98, American Society of Civil Engineers, pp. 349-358.

Ransom, B.H., Steig, T.W., (1995), "Comparison of the Effectiveness of Surface Flow and Deep Spill for Bypassing Pacific Salmon Smolts (*Oncorhynchus spp.*) at Columbia River Basin Hydropower Dams", Technical Paper, ASCE Waterpower 95.

Ruggles, C.P. and Murray, D.G., (1983), "A Review of Fish Response to Spillways", Canadian Technical Report of Fisheries and Aquatic Sciences, No. 1172.

Sinha, S.K., (1996), "Three-Dimensional Numerical Model for Turbulent Flows Through River Reaches of Complex Bathymetry" Ph.D. Dissertation, University of Iowa.

Sinha, S.K., Sotiropoulos, F., Odgaard, A.J., (1995), "A Multiblock Numerical Model for Natural Rivers", Technical Paper, ASCE Waterpower 95.

Sinha, S.K., Sotiropoulos, F., Odgaard, A.J., (1996), "Numerical Model Studies for Fish Diversion at Wanapum/Priest Rapids Development. Part I: Three-Dimensional Numerical Model for Turbulent Flows Through Wanapum Dam Tailrace Reach" IIHR Report No. 250, Iowa Institute of Hydraulic Research, University of Iowa.

Sverdrup report, (1995), "A review of the 1981 to 1992 Hydroacoustic Studies of the Wells Dam Juvenile Fish Bypass System", Sverdrup Corporation, June.

Sweeney, C.E., Weitkamp, D.E., (1995), "Surface Attraction Fish Bypass at Rocky Reach Dam", Technical Paper, ASCE Waterpower 95.

Thomas, S., US Army Corps of Engineers, North Pacific Divison, "Columbia River and Salmon – A Brief History", Snake and Columbia River Fish Programs, Special Issue.

US Army Corps of Engineers, North Pacific Division, (1994), "Surface-Oriented Bypasses for Juvenile Fish", Salmon Passage Notes, Snake and Columbia River Fish Programs, November.

US Army Corps of Engineers, North Pacific Division, (1998), "Evaluating Technologies for Imporved Fish Passage", Salmon Passage Notes, Snake and Columbia River Fish Programs, January.

US Army Corps of Engineers, Walla Walla District, (1997), "Water Velocity Measurement Data Using an Acoustic Doppler Velocimeter (ADV) at Lower Granite Dam in 1999", Final Draft Report, Battelle Laboratories.

Welch, T.J., (1997), "Perspectives on Surface-Oriented Fish Diversion Systems at FERC-Licensed Projects", Fish Passage Workshop, Milwaukee, WI.

APPENDIX A
GENERAL DETAILS OF LOWER GRANITE DAM

General		
Location:		
State		Washington
County		Garfield and Whitman
River		Snake
River Mile		107.5
Township		14 N
Range		43 E
Section		32
Latitude		46° 39' 37"
Longitude		117° 25' 37"
River miles from mouth of Snake River		107.5
River miles upstream of Little Goose Dam		37.2
Ownership and Purpose:		
Owner	U.S. Army Corps of Engineers, Walla Walla District	
Type of plant	Run-of-river	
Authorized purpose	Power generation and inland navigation	
Other uses	Flood control (maintain levee freeboard at Lewiston), fishery and recreation	

Levees		
Materials	Gravel and earth fill with impervious core	
Dimensions (feet):		
Top width		12
Top elevation (above backwater profile for standard project flood)		5
Slopes:		
Waterside		1V on 2H
Landside		1V on 2H
Lewiston Levees:		
Embankment length (miles)		8.6
Installed pumping capacity (cfs)		450.4

Table A.1 Pertinent geometric and operational data for Lower Granite Lock and Dam.

Dam (General)	
Axis (Lambert)	N 32° 00'E
Dimensions (feet):	
Dam total crest length	3,200
North abutment embankment length	1,435
Spillway to powerhouse non-overflow length	43.4
Spillway to navigation lock non-overflow length	43.4
Maximum overall concrete height (powerhouse sump deck to deck)	254
Maximum non-overflow monolith concrete heights:	
North	151
Central	166
South	181
Maximum lock wall monolith concrete height (culverts to deck)	191
Deck Elevations (feet above mean sea level):	
Non-overflow sections and upstream end of navigation lock	751
Downstream end of navigation lock	746
South shore fish ladder and fishwater intake	656

Reservoir	
Name	Lower Granite Lake
Distances (miles):	
Length of Snake River to Asotin dam site (RM 146.8)	39.3
Length to Clearwater River	4.6
Length of shoreline	91
Average width	0.3
Maximum width	0.6
Depth (feet):	
Normal high pool to tailwater elevation under low flow condition (30,000 cfs or less)	100
Elevations (feet above mean sea level):	
Maximum at dam for spillway design flood	746.5
Normal operating range at confluence gage (RM 139.5)	733 - 738
Minimum at dam for standard project flood	724
Surface Area (acres):	
At elevation 738 feet (low flow, flat pool)	8,900
Storage Capacity (acre-feet):	
Below flat pool elevation 733 feet	440,200
Below flat pool elevation 738 feet	483,800
Between flat pool elevations 733 and 738 feet	43,600

Table A.1 Continued.

Powerhouse	
Number of Units:	
Complete units installed initially	3
Skeleton units installed initially	3
Total units currently installed	6
Plant power capacity (nameplate rating in kilowatts)	810,000
Dimensions (feet):	
Overall length	656
Overall width (transverse section)	243.17
Maximum height (draft tube invert to intake deck)	228
Spacing:	
Units 1 through 5	90
Unit 6	96
Erection and service bay	110
Elevations (feet above mean sea level):	
Intake deck elevation	751
Tailrace deck elevation	656
Turbines:	
Type	Kaplan, 6-blade
Runner diameter (inches)	312
Revolutions per minute (RPM)	90
Rating (horsepower)	212,400
Distributor centerline elevation (feet above mean sea level)	599
Generators:	
Nameplate rating (kilowatts)	135,000
Power factor	0.95
Kilovolt-ampere rating	142,100
Crane Capacities (tons):	
Intake gantry (joint use with spillway)	100
Bridge	600
Draft tube gantry	50

Spillway	
Number of bays	8
Maximum design capacity (cfs)	850,000
Dimensions (feet):	
Overall length (abutment centerlines)	512
Stilling basin length	188

Table A.1 Continued.

Elevations (feet above mean sea level):	
Deck elevation	751
Ogee crest elevation	681
Flip lip elevation	630
Stilling basin elevation	580
Control Gates:	
Type	Tainter
Dimensions (feet):	
Width	50
Height	60

Navigation Lock and Channels	
Lock Dimensions (feet):	
Overall width at foundation	304
Overall width at deck	186
Chamber net clear length	674
Chamber net clear width	86
Maximum depth over sills	20.0
Minimum depth over sills	15.0
Lock Elevations (feet above mean sea level):	
Minimum tailwater elevation	633.0
Upper lock sill elevation	718.0
Lower lock sill elevation	618.0
Lock Gates:	
Upstream gate:	
Type	Submersible tainter
Height (feet)	23
Downstream gate:	
Type	Miter
Height (feet)	122
Approach Channels:	
Length of guide-walls from face of gate (feet):	
Upstream (floating)	750
Downstream	700
Downstream approach channel:	
Width (feet)	250
Bottom elevation (feet above mean sea level)	617
Lock Operation:	
Maximum operating lift (feet)	105
Operating water surface elevations in chamber (feet amsl)	633 - 738

Table A.1 Continued.

Abutment Embankment	
Materials	Gravel fill with rock facing, impervious silt core with combination sand and gravel filters
Dimensions (feet):	
Embankment top width	45
Elevations (feet above mean sea level):	
Embankment top elevation	756
Slopes:	
Upstream	1V on 2H
Downstream	1V on 2H

Fish Facilities	
Upstream Migrants Fish Ladders:	
Number of fish ladders	1
Design capacity (cfs)	75
Ladder clear width (feet)	20
Slopes:	
Weir 634 to Weir 627	1V on 10 H
Weir 728 to Weir 737	1V on 32H
Main Exit Channel:	
Location	Between weir 737 and pool in non-overflow section
Top of trashrack elevation	732
Invert elevation	727
Width (feet)	6
Alternative Exit Channel:	
Location	Pool elevation below 727
Exit pipe to reservoir	18-inch-diameter full plastic pipe down to El. 718, and a half-round plastic pipe down to El. 710
Operating Elevations (feet above mean sea level):	
Design pool range	733 - 738
Maximum pool range	732 - 739
Design tailwater range	633 - 642
Maximum tailwater range	633 - 645.4
Operating River Flow (cfs):	
Design range	0 - 225,000
Maximum range	0 - 340,000

Table A.1 Continued.

Pumps for fishway system attraction water:	
Number of pumps	3
Capacity (cfs)	3,150
Number of adult fish trap and handling facilities	1
Downstream Migrants Bypass System:	
Number of extended-length submerged bar screens	18
Number of vertical barrier fish screens	18
Design capacity (cfs)	200 - 250
Operating Elevations (feet above mean sea level):	
Design pool range	733 - 738
Orifices from bulkhead and fish screen slots:	
Sizes (diameter in inches)	10, 12
Number of each size	36, 36
Number of fingerling collection galleries	1
Number of fingerling transportation pipes	1
Number of fingerling holding and sampling facilities	1
Number of fingerling transportation facilities:	
Truck loading	1
Barge loading	1

Hydrologic Data	
(Based on stream flow data for the Snake River near Clarkston, Washington)	
Drainage Area (square miles)	103,200
Period of Record	October 1915 to September 1972 (Discontinued in December 1972)
Recorded Discharges (cfs):	
Instantaneous maximum, 29 May 1948	369,000
Instantaneous minimum, 2 September 1958	6,660
Average annual flow	50,300
Average annual mean daily peak flow	188,300
Extreme Discharges Beyond Record (cfs):	
Flood of June 1894 (actual)	409,000
Flood of June 1894 (controlled by existing projects)	295,000
Standard Project Flood with Existing Projects (cfs):	
Snake River below Clearwater River	420,000
Snake River above Clearwater River	295,000
Clearwater River above Snake River	150,000

Table A.1 Continued.

APPENDIX B
CALIBRATION AND VALIDATION DATA AND RESULTS

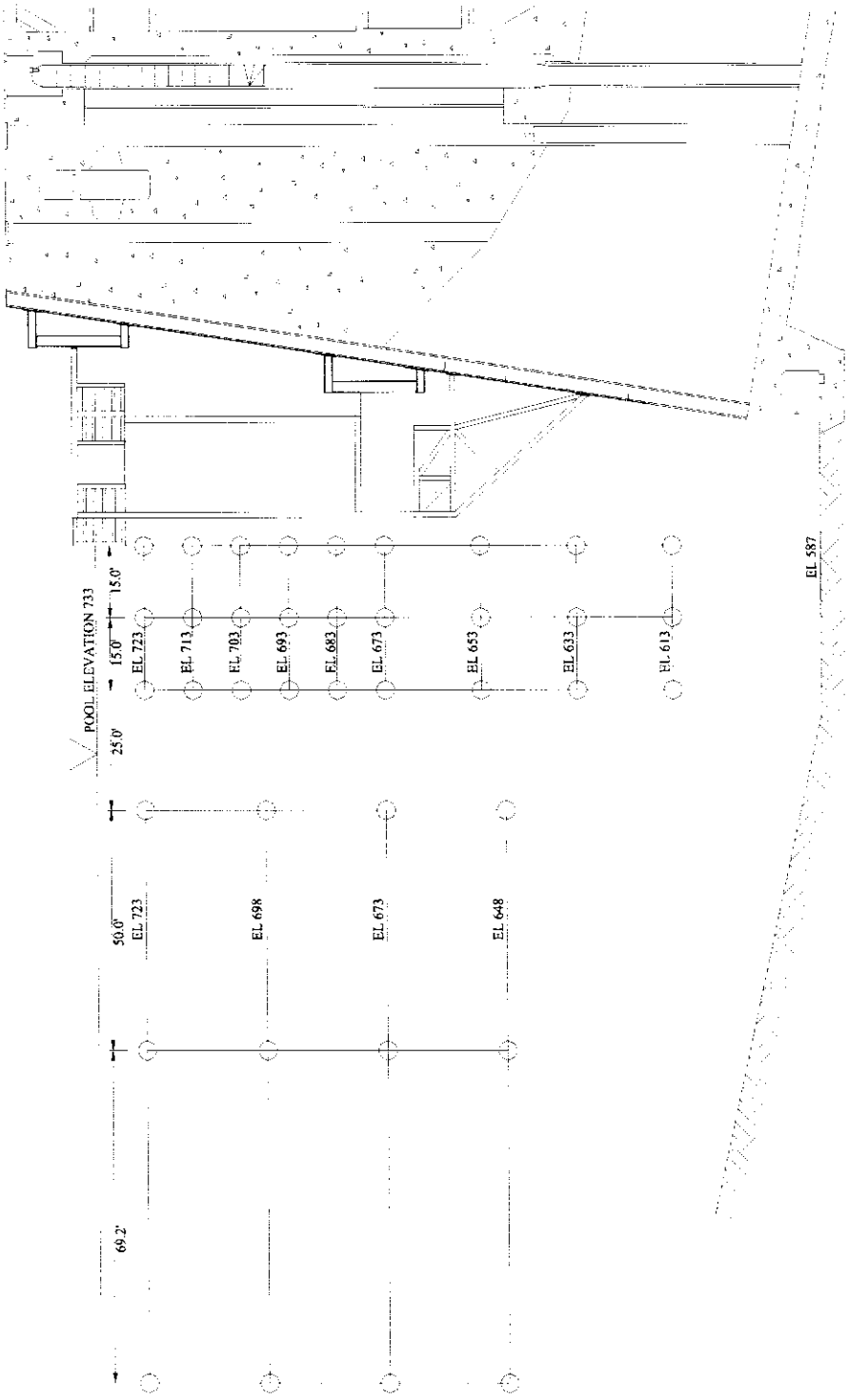

Figure B.1 Calibration and validation data set collection location - Vertical plane.

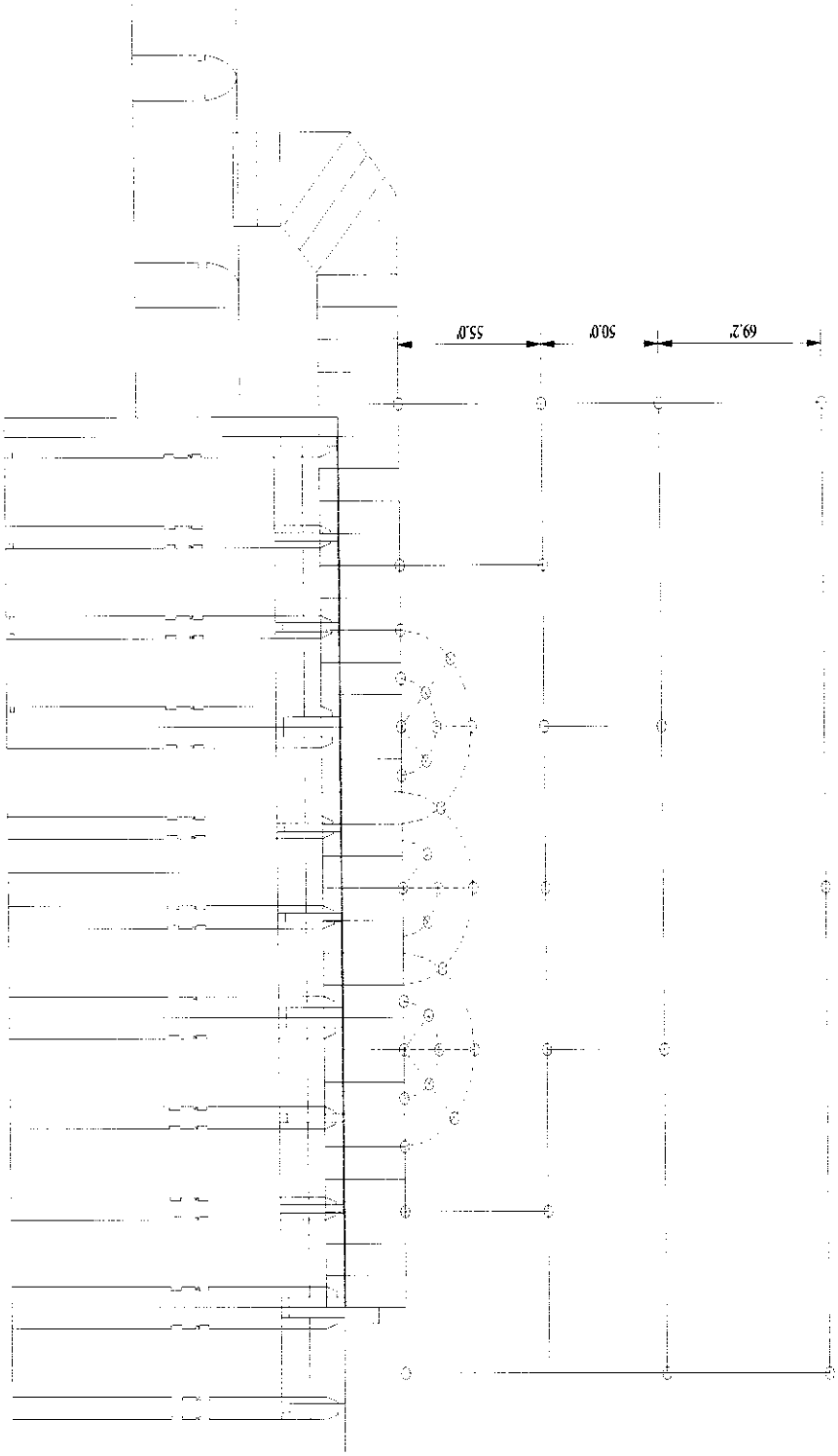

Figure B.2 Calibration and validation data set collection location - Horizontal plane.

State Plane Coordinates (ft)		Elevation	Velocity Component (ft/s)		
East	North	(ft)	Vx	Vy	Vz
498282.4	2770834.1	723.0	1.290	1.152	0.509
498255.9	2770876.5	723.0	0.887	0.033	0.886
498245.3	2770893.5	723.0	0.743	0.026	0.743
498237.3	2770906.2	723.0	0.793	0.050	0.791
498229.3	2770918.8	723.0	0.725	0.134	0.712
498221.3	2770931.6	723.0	0.912	0.008	0.912
498213.4	2770944.3	723.0	0.773	0.042	0.772
498202.8	2770961.2	723.0	0.555	0.100	0.543
498192.2	2770978.3	723.0	0.535	0.101	0.503
498184.3	2770991.0	723.0	0.775	0.094	0.768
498176.3	2771003.7	723.0	0.885	0.153	0.872
498168.3	2771016.4	723.0	1.010	0.104	0.998
498160.4	2771029.1	723.0	0.898	0.066	0.895
498149.8	2771046.1	723.0	1.068	0.054	1.066
498123.3	2771088.5	723.0	0.869	0.030	0.869
498244.0	2770915.6	723.0	0.839	0.592	0.479
498232.7	2770933.6	723.0	0.443	0.265	0.236
498217.5	2770958.0	723.0	0.915	0.629	0.607
498206.2	2770976.0	723.0	0.950	0.673	0.571
498191.0	2771000.4	723.0	0.899	0.591	0.472
498179.7	2771018.4	723.0	0.560	0.258	0.354
498242.1	2770926.9	723.0	0.897	0.699	0.441
498215.6	2770969.3	723.0	0.948	0.729	0.545
498189.1	2771011.7	723.0	0.755	0.463	0.428
498230.1	2770949.0	723.0	0.576	0.344	0.298
498203.6	2770991.4	723.0	0.941	0.665	0.568
498258.6	2770912.2	723.0	0.943	0.728	0.452
498183.1	2771033.0	723.0	0.682	0.245	0.440
498254.8	2770934.8	723.0	1.024	0.826	0.505
498228.2	2770977.3	723.0	0.829	0.578	0.485
498201.7	2771019.7	723.0	1.032	0.817	0.538
498329.0	2770863.3	723.0	1.255	1.174	0.412
498302.5	2770905.7	723.0	1.129	0.984	0.535
498276.0	2770948.1	723.0	1.245	1.074	0.612
498249.5	2770990.5	723.0	1.016	0.854	0.481
498223.0	2771032.9	723.0	1.281	0.994	0.799
498196.5	2771075.3	723.0	1.062	0.716	0.764
498170.0	2771117.7	723.0	0.491	0.212	0.421
498371.4	2770889.8	723.0	1.264	1.187	0.427
498318.4	2770974.6	723.0	1.264	1.096	0.625

Table B.1 Calibration data set under 1997 geometric and flow conditions.

State Plane Coordinates (ft)		Elevation	Velocity Component (ft/s)		
East	North	(ft)	Vx	Vy	Vz
498265.4	2771059.4	723.0	1.374	1.105	0.815
498212.4	2771144.2	723.0	1.272	0.872	0.925
498430.1	2770926.5	723.0	1.280	1.219	0.387
498350.6	2771053.7	723.0	1.249	1.065	0.653
498271.1	2771180.9	723.0	1.117	0.787	0.781
498282.4	2770834.2	698.0	1.475	1.287	0.574
498255.9	2770876.6	698.0	0.839	0.287	0.348
498149.8	2771046.1	698.0	1.217	0.267	1.041
498123.3	2771088.5	698.0	1.130	0.317	0.887
498329.0	2770863.3	698.0	1.449	1.283	0.623
498302.5	2770905.7	698.0	1.401	1.138	0.744
498276.0	2770948.1	698.0	1.370	1.096	0.762
498249.5	2770990.5	698.0	1.455	1.037	0.947
498223.0	2771032.9	698.0	1.484	1.046	1.009
498196.5	2771075.3	698.0	1.489	0.904	1.127
498170.0	2771117.7	698.0	1.456	0.751	1.199
498371.4	2770889.8	698.0	1.428	1.281	0.616
498318.4	2770974.6	698.0	1.421	1.211	0.736
498265.4	2771059.4	698.0	1.512	1.124	1.003
498212.4	2771144.2	698.0	1.301	0.822	0.995
498430.1	2770926.5	698.0	1.355	1.215	0.601
498350.6	2771053.7	698.0	1.413	1.145	0.827
498271.1	2771180.9	698.0	1.446	0.981	1.056
498282.4	2770834.2	673.0	1.760	1.511	0.731
498255.9	2770876.6	673.0	2.018	1.589	0.320
498245.3	2770893.5	673.0	2.013	1.444	0.240
498237.3	2770906.2	673.0	2.009	1.248	0.308
498229.3	2770918.9	673.0	1.967	1.151	0.356
498221.3	2770931.7	673.0	1.890	1.180	0.508
498213.4	2770944.3	673.0	1.950	1.305	0.551
498202.8	2770961.3	673.0	2.015	1.331	0.722
498192.2	2770978.2	673.0	1.984	1.352	0.453
498184.3	2770991.0	673.0	1.997	1.231	0.268
498176.3	2771003.7	673.0	2.005	1.003	0.363
498168.3	2771016.5	673.0	1.882	1.041	0.453
498160.4	2771029.1	673.0	2.078	1.229	0.868
498149.8	2771046.1	673.0	2.011	1.312	0.970
498123.3	2771088.5	673.0	1.525	0.554	1.158
498244.0	2770915.5	673.0	1.985	1.482	0.871
498232.7	2770933.6	673.0	1.826	1.279	0.914

Table B.1 Continued.

State Plane Coordinates (ft)		Elevation	Velocity Component (ft/s)		
East	North	(ft)	Vx	Vy	Vz
498217.5	2770957.9	673.0	1.993	1.419	1.038
498206.2	2770976.0	673.0	2.029	1.475	1.065
498191.0	2771000.3	673.0	1.887	1.088	1.110
498179.7	2771018.4	673.0	1.976	1.231	1.113
498242.1	2770926.9	673.0	1.821	1.372	0.848
498215.6	2770969.3	673.0	1.861	1.362	0.963
498189.1	2771011.7	673.0	1.911	1.280	1.084
498230.1	2770949.0	673.0	1.792	1.286	0.925
498203.6	2770991.4	673.0	1.895	1.296	1.133
498258.6	2770912.2	673.0	1.825	1.431	0.858
498183.1	2771033.0	673.0	1.896	1.271	1.200
498254.8	2770934.8	673.0	1.736	1.332	0.941
498228.2	2770977.3	673.0	1.776	1.302	1.022
498201.7	2771019.7	673.0	1.710	1.139	1.064
498329.0	2770863.3	673.0	1.561	1.351	0.718
498302.5	2770905.7	673.0	1.563	1.335	0.749
498276.0	2770948.1	673.0	1.578	1.266	0.838
498249.5	2770990.5	673.0	1.653	1.262	0.986
498223.0	2771032.9	673.0	1.689	1.173	1.139
498196.5	2771075.3	673.0	1.599	1.035	1.143
498170.0	2771117.7	673.0	1.654	0.927	1.322
498371.4	2770889.8	673.0	1.464	1.290	0.676
498318.4	2770974.6	673.0	1.556	1.284	0.869
498265.4	2771059.4	673.0	1.525	1.116	1.025
498212.4	2771144.2	673.0	1.480	0.932	1.126
498430.1	2770926.5	673.0	1.336	1.236	0.508
498350.6	2771053.7	673.0	1.425	1.129	0.866
498271.1	2771180.9	673.0	1.435	0.972	1.051
498282.4	2770834.2	672.0	1.939	1.739	0.721
498255.9	2770876.6	672.0	1.971	1.762	0.702
498149.8	2771046.1	672.0	2.252	1.785	1.137
498329.0	2770863.3	672.0	1.640	1.458	0.672
498302.5	2770905.7	672.0	1.717	1.424	0.898
498276.0	2770948.1	672.0	1.707	1.364	0.947
498249.5	2770990.5	672.0	1.744	1.343	1.030
498223.0	2771032.9	672.0	1.722	1.205	1.161
498196.5	2771075.3	672.0	1.771	1.094	1.325
498170.0	2771117.7	672.0	1.704	0.921	1.352
498371.4	2770889.8	672.0	1.460	1.289	0.642
498318.4	2770974.6	672.0	1.589	1.237	0.975

Table B.1 Continued.

APPENDIX C
1998 NEAR-FIELD MODEL RESULTS

APPENDIX D
1999 MODEL RESULTS